Characterisation of peripheral neuropathy and neuronal and endothelial markers of neuropathic pain: A comparative study across preclinical models of neuropathic pain

William Blackstone Whines

Dr Lisa Lione, Dr Shoib Siddiqui

September 2022

Submitted to the University of Hertfordshire in partial fulfilment of the requirements of the degree of MSc by Research

Abstract

Neuropathic pain is pain caused by a lesion or disease to the somatosensory pathways. A leading cause is diabetic peripheral neuropathy which effects over half of all diabetic patients. This neuronal damage commonly leads to sensory disturbances such as dysesthesia, allodynia, and hyperalgesia. These unpleasant sensory experiences are often accompanied by secondary symptoms such as anxiety and depression; all of which negatively effects the suffers quality of life. The underlying pathology behind diabetic peripheral neuropathy and other neuropathic pain conditions is not well understood and requires further elucidating. The lack of understanding poses significant problems for diagnosis and optimal treatment strategies, resulting in only a small proportion of sufferers benefitting from current pharmacological treatment. Without biomarkers that can accurately predict neuropathy and neuropathic pain, it is hard to successfully identify preclinical treatments that will translate to optimal treatment strategies for neuropathic pain sufferers. Potential biomarkers of peripheral neuropathic pain include intra-epidermal nerve fibre density (IENFD), Langerhans cells (LCs) density, calcitonin gene-related peptide (cGRP) and vascular endothelial growth factor (VEGF). Plantar skin biopsies were collected from male Wister Han ISG STZ-induced type 1 diabetic rats with a stable mechanical allodynia after 7 weeks and from male and female high fat diet (HFD) induced type diabetic C57 BI6 mice. An immunohistochemistry (IHC) protocol was developed to quantify IENFs, LCs and cGRP density using anti PGP 9.5 and cGRP antibodies. There was found to be a significant decrease in IENF density in STZ induced type 1 diabetic rats at 2- ($p<0.001$), and 7- weeks ($p<0.001$) which correlated with an increase in LC expression ($r= -0.6214$, $p= <0.002$). There was also a proportional increase in cGRP expression in STZ induced type 1 diabetic rats at 2-, 4-, and 7-weeks, the increase was only significant at 2 weeks ($p=0.012$). No time course effects in IENFD decrease, LCs increase, or cGRP increase were found in 2-, 4-, and 7-week STZ induced type 1 diabetic rats. VEGF expression levels were quantified, using western blot, in control and STZ induced type 1 diabetes rat retina however no signal was produced with the anit-VEGF antibody, suggesting an issue with the antibody or protocol. In the HFD induced type 2 diabetes model there was a significant decrease in IENFD between male mice fed control chow and those fed 60% fat diet ($p < 0.001$) as well as between male mice fed 42% and 60% fat diet ($p=0.010$). In female mice there was a significant decrease in IENFD from the control chow group in both the 42% fat diet group ($p=0.002$) and the 60% fat diet group ($p < 0.001$). However no significant change was found in LC expression or proportional levels of cGRP in the HFD induced type 2 diabetes model. This study demonstrated that the quantification of IENFD can be reliably and comparatively measured in plantar skin of healthy and diabetic type 1 and 2 neuropathic rodents. The observed increase in LC expression levels in combination with IENFD have the potential to assess the development and potential severity of the neuropathy, as well as predict the extent of neuropathic pain. The use of CGRP as a reliable biomarker was inconclusive in this study however further investigation is warranted into its use as a translatable neuropathy biomarker, as well as the role it plays in the generation of neuropathic pain, and mechanism for analgesia.

Acknowledgments

First and foremost, I would like to extend my thanks to my supervisors Dr Lisa Lione and Dr Shoib Siddiqui for their endless support, guidance, and patience throughout this project. Their support made the entire project possible and has helped transition into a better researcher.

I would also like to thank my fellow colleagues and lab members for their general assistance throughout the project. Especially to Michael Lanigan who helped at every step and seemingly never became tiered of the endless questions.

I would also like to extend my thanks to Komal Patel, Yugal Kalaskar, Alex Gant, Diana Francis, and the rest of the laboratory technical staff for their constant advice and assistance during the project period.

Finally, I would like to acknowledge University of Hertfordshire for allowing me access to their facilities which enabled me to complete this work.

Contents

1. Introduction

1.1 Pain pathway (nociception)

Pain, as defined by the International Association for the Study of Pain (IASP), is ‘‘an unpleasant sensory and emotional experience associated with actual or potential tissue damage” (Vader et al., 2021). It is an evolutionary trait which all humans experience that serves to protect individuals from harm. In the short-term acute pain causes the individual to remove themselves from the tissue damaging noxious stimuli, curtailing, and preventing further tissue damage, and allowing the affected area to heal. Under normal conditions pain is a direct response to an event causing tissue damage such as injury, inflammation, or cancer. In the periphery, pain is transduced by nociceptors, which are located on small diameter primary afferent neurones sensitive to mechanical, thermal, and chemical stimuli (Julius & Basbaum, 2001). The two main types of small sensory nerve fibres in the periphery are C and Aδ fibres. C fibres (blue pathway in figure 1) are unmyelinated, and the majority have polymodal sensory endings which evoked a poorly localised, dull, burning type pain, whereas Aδ fibres (red pathway figure 1) are partially myelinated and are associated with a highly localised sharp, shotting pain (Dubin & Pataoutian, 2010). Theses primary afferent sensory fibers, also called first order neurones, have their cell body in the dorsal root ganglion (DRG) and synapse into the spinal cord at the dorsal horn in a region known as the substantia gelatinosa, where they release glutamate and substance P as well as neuropeptides such as calcitonin gene-related peptide (cGRP). From the dorsal horn second order neurones decussate and ascend along the spinothalamic tract through the spinal cord and brain stem into the ventral and medial parts of the thalamus (double blue line figure 1). From which third order neurones travel to specific regions in the somatosensory cortex where pain is perceived. This ascending pathway is modulated by a descending pathway where neurones arrive from the periaqueductal grey (PAG) matter area of the mid brain and synapse with a second neuron in the rostral ventromedial medulla (RVM) in the medulla (black line figure 1). This is a serotonergic/noradrenergic neuron which descends into the dorsal horn inhibiting the synapse between the first order and second order neurons of the ascending pathway. Serotonin and noradrenaline will bind and activate receptors at the presynaptic junction inhibiting release of substance P/glutamate. It also stimulates interneurons, mainly GABAergic, in the dorsal horn to release endogenous opioids such as enkephalin, further inhibiting the release of substance P/glutamate from the presynaptic first order neuron and blocking ascending pain transmission signals.

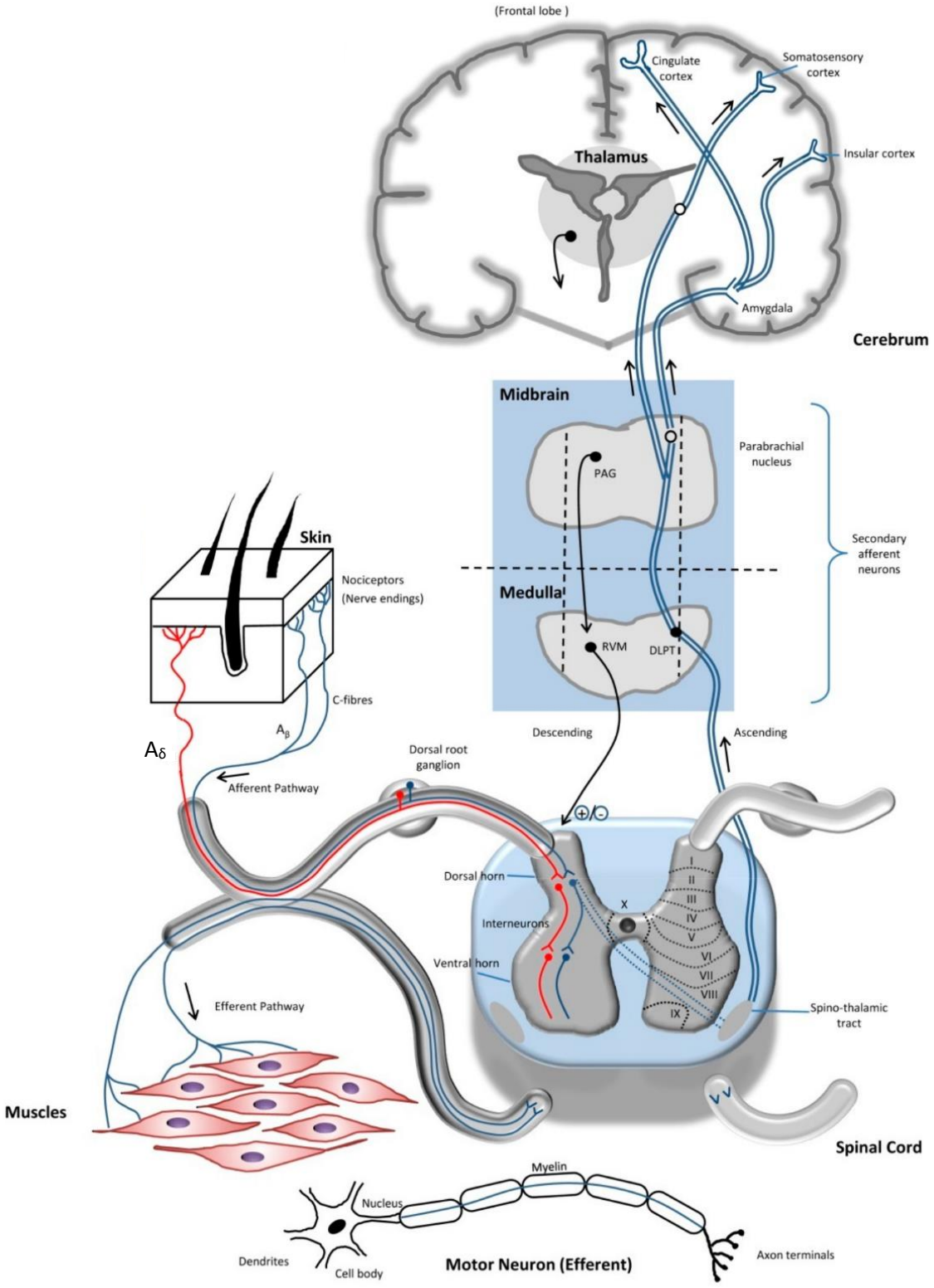

Figure 1. Route of pain transmission through the ascending and descending order nerve fibres after stimulation from a noxious stimuli in the periphery, and synaptic transmission in the synaptic cleft (image taken from Yam et al., 2018)

1.2 Neuropathic pain (NP): Modulation in pain pathway

When pain persists with no clear reason, it becomes chronic and serves no protective purpose. Chronic pain, as defined by the ISAP, is pain which persists or recurs for longer than 3 months (Treede, 2019). Neuropathic pain (NP) is pain caused by an injury or disease to the somatosensory pathway as defined by the International Association for the Study of Pain (Merskey, 1986). It can be thought of pain as a disorder to neuronal function rather than a normal physiological response to tissue injury. Whereby pain generation persist unrelated to any peripheral tissue injury. This can occur centrally following e.g. a stroke or multiple sclerosis, or peripherally e.g. nerve damage caused by mechanical injury or diabetic peripheral neuropathy. NP is associated with a wide range of conditions, and is highly prevalent within society, being represented in 7-10% of the population (Derry et al., 2019). In the general population, the incidence of NP is difficult to accurately estimate due to varying definitions and disagreement on classifications but has been found to be more prolific among women and in those with labour intensive jobs. The underlying mechanisms of NP are not fully understood, and many are yet to be elucidated. In many instances, one mechanism can underlie multiple symptoms, with the same symptoms being caused by different mechanisms in different patients, and the mechanisms changing temporally (Woolf, & Mannion, 1999). Although much evidence supports that over expression of voltage gated sodium channels can cause spontaneous activity in damaged sensory neurones (Lai, Porreca, Hunter, & Gold, 2004). The sympathetic nervous system may also play a role as α-adrenoreceptors can become overexpressed on the damaged sensory neurons causing them to develop a hypersensitivity to noradrenaline. Leading to severe pain.

Chronic NP which outlasts the tissue injury, arises from dysfunction of the normal physiological nociceptive pathway. Leading to unpleasant abnormal sensations known as dysesthesia, allodynia (pain caused by a usually non-painful stimuli), hyperalgesia (the increased pain sensation from a painful stimulus), aftersensations, (continued pain after the stimuli has gone), hyperpathia (where the reaction to a painful stimulus is increased, especially to repeated stimulation), or spontaneous pain without any precipitating stimulus (Colloca et al., 2017). All these symptoms are unpleasant sensory experiences, with sensations often being described as electric shock like, burning, shooting, prickly, pins and needles, squeezing, or freezing (Colloca et al., 2017). Along with physical symptoms there are often accompanying secondary symptoms including poor quality of sleep, anxiety, and depression. All of which reduce the sufferer's quality of life compounded with higher rates of unemployment and a decrease in productivity levels putting a further burden on the patient's life.

There are several molecular mechanisms which underlie NP induced mechanical allodynia and hyperalgesia. Damaged primary sensory afferent nerve fibres develop altered sodium channel expression (especially $Na_V1.3$, $Na_V1.7$, $Na_V1.8$, and $Na_V1.9$) and spontaneous ectopic activity increase peripheral input and sensitisation (von Hehn, Baron, & Woolf, 2012). Peripheral sensitisation acts as a driving force (wind up) for central sensitisation, causing an increase in the level of pain as well as pain persisting after the noxious stimuli has gone. Many signalling molecules are thought to contribute to sensitisation (figure 2). Substance P and cGRP are secreted by the primary afferent fibers. Substance P acts on mast cells, releasing histamine and other mediators, whilst cGRP is a potent vasodilator, both of which promote inflammation. This mechanism is known as neurogenic inflammation, it amplifies and sustains the inflammatory reaction and the accompanying activation of nociceptive afferent fibres. Along with cGRP and substance P, nerve growth factor (NGF), brain derived neurotrophic factor (BDNF), and many other mediators are implicated in central facilitation of sensitisation (Ji, Kohno, Moore, & Woolf, 2003). The upregulation of genes and expression levels of these inflammatory mediators facilitate synaptic transmission in the dorsal horn. Synaptic

strength is also increased postsynaptically due to increased activity in NMDA, AMPA, and glutamate receptors (von Hehn, Baron, & Woolf, 2012). Ultimately, the result of these maladaptive mechanisms following damage to the peripheral nerve fibres causes dysfunctional signalling from the first order afferent neuron to the second order neurones, with impaired transduction and transmission.

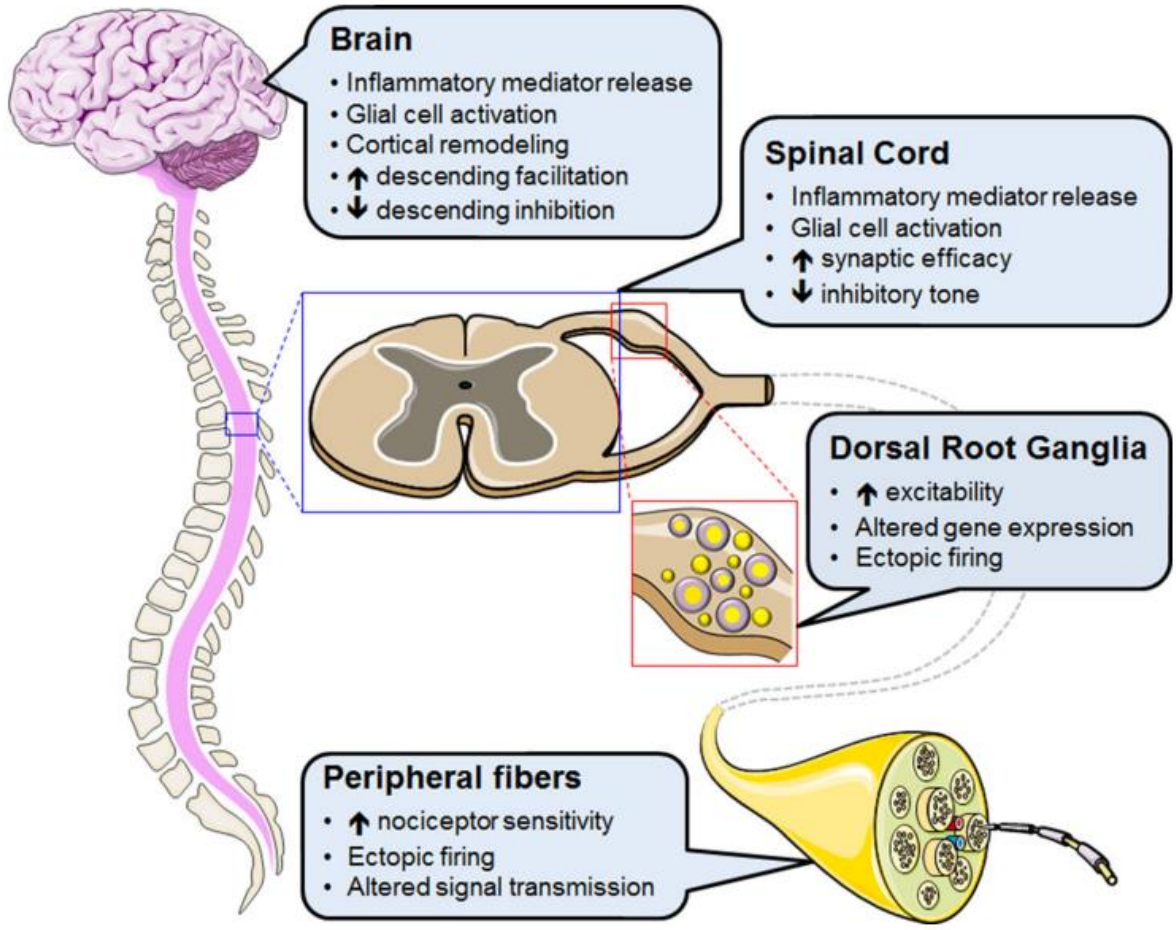

Figure 2. An overview of peripheral and central changes contributing to neuropathic pain (image taken from Meacham et al., 2017)

1.3 Peripheral Neuropathy (PN)

Neuropathy is disease or dysfunction to one or more peripheral nerves, causing loss of sensory function from the affected nerve fibres, and is often the starting point for neuropathic pain. Peripheral neuropathy (PN) is caused by damage to the nervous system running from peripheral nociceptive terminals to the dorsal root horn (figure 1), with pain being the most the common symptom. A common cause of PN is diabetes with diabetic peripheral neuropathy (DPN) affecting over half of all diabetics, and 30% of these experiencing painful peripheral neuropathy (Abbott, Malik, van Ross, Kulka-rni, & Boulton, 2011). There are two main types of diabetes, type 1 and type 2. Type 1 is a genetic condition developing early in life, whilst type 2 is largely lifestyle based and develops over time. Type 2 is far more prevalent then type 1 affecting 90% of those with diabetes compared to around 8% who have type 2 (about 2% of people with diabetes have rarer forms). Although the precise mechanisms by which diabetes generates neuropathy is/are not fully

understood, recent advances in this area have been made. Two hallmarks of type 1 and 2 diabetes are hyperglycaemia and hyperlipidaemia. Through a variety of mechanisms, these can impair peripheral nerve function and cause neuronal changes; resulting in demyelination of axonal fibres, particularly to Aβ and Aδ fibres, which subsequently leads to axonal loss peripherally and a reduction in nerve fibre density distally. Additionally, diabetes causes microvascular damage and a reduction in neural trophic support, both nerve growth factor (NGF) and vascular endothelial growth factor A (VEGF-A) are reduced (Hulse et al., 2015). Leading to reduced blood flow to the nerves, in turn causing hypoxia which also impairs nerve function. It is unknown as to why some diabetic patients develop painful neuropathies and others don't, which illustrates the complexity of the underlying mechanisms of the disease and the need for an objective and robust pain biomarker.

1.4 Neuropathic pain treatment and its limitations: Poor translatability

Management of neuropathic pain is met with many challenges due to the underlying cause(s) and specific mechanism(s) often being unknown, therefore treatment options are mainly limited to focusing on managing the symptoms of the pain and etiological features (Cavalli, Mammana, Nicoletti, Bramanti, & Mazzon, 2019). Diabetic patients are advised to monitor their blood glucose levels closely to maintain optimal glycaemic control to mitigate the hyperglycaemic environment. The IASP as well as the Special Interest Group of Neuropathic Pain recommend tricyclic antidepressants, and anti-epileptics including selective serotonin-norepinephrine reuptake inhibitors (SNRIs) (venlafaxine and duloxetine) and gabapentinoids (pregabalin, gabapentin) respectively. These are also recommended as first line interventions by the UK National Institute for Health and Care Excellence (NICE) (NICE, 2013). Gabapentin and pregabalin (gabapentinoids) are ligands of the $\alpha_2\delta$ calcium channel subunit which is connected to the main α_1 subunit of voltage-gated calcium channels (Risher & Eroglu, 2020). They disrupt the function of the $\alpha_2\delta$ subunit and the proteins it interacts with, thereby inhibiting excitatory transmitter release (Calandre, Rico-Villademoros, & Slim, 2016). SNRIs and tricyclic antidepressants inhibit serotonin and noradrenaline reuptake in the descending pathway, inhibiting and suppressing the ascending pain pathway (Grandoso, Pineda & Ugedo, 2004; Hunzikez et al., 2005). Topical treatments include capsaicin and lidocaine are used for people with localised neuropathic pain who can't tolerate oral medications or wish to avoid them (NICE, 2013). Capsaicin patches in high concentration (Qutenza 8% capsacin patch) activates and desensitises TRPV1, potential reversing degeneration of epidermal nerve fibres and improving NP (Nolano et al., 1999). Lidocaine is a topical local anaesthetic of the amino acid type and has shown potential as a NP treatment (Derry et al., 2014). Tramadol along with strong full agonist opioids like morphine and oxycodone, are not recommended as first or second line treatment of NP but are sometimes used to treat sudden onset of serve pain and if acute therapy is needed (NICE, 2013). Botulinum toxin-A (botox) is a neurotoxin causing localised destruction of hypersensitive afferent nerve fibres which may be helpful in localised PN (Mittal, Safarpour & Jabbari, 2016).

Due to the underlying mechanism**s** and pathologies of NP being poorly understood, few patients benefit from current treatments and medication (for review see Fisher, Lanigan, Upton, & Lione, 2021). This is highlighted by the fact the most extensively studied drug across NP conditions, pregabalin, benefits less than half of those treated with it (Derry, 2019). In painful diabetic peripheral neuropathy only around a third of treated patients experience 50% pain relief (Jensen et al., 2006). Current treatments are also accompanied with an array of adverse side effects. This compounded with the poor efficacy of the treatments means that the management of NP is not adequately met and there is a gulf to be filled before it becomes satisfactory. Novel medications along with treatments for other pain conditions have been studied in preclinical animal models, in

addition to phase 2 and 3 clinical trials, however none of these have come to fruition as an effective NP treatment. A large contributing factor to this is that pain and nociception are different phenomena, pain cannot solely be inferred form sensory neurons. As the perception of a noxious stimuli (nociception) does not equate to pain per se, due to the fact pain is a deeply subjective experience which comprises a psychological *and* emotional component. With the IASP defining pain as an unpleasant sensory and emotional experience associated with actual or potential tissue damage (Raja et al., 2020). The extent to which someone perceives pain to a specific stimulus is dependent on a host of factors independent to the stimuli itself. This includes genetic, developmental, social, and psychological factors. For example, the situational and emotional factors that are present when the pain is experienced, can dramatically alter the intensity of the pain perception. It is also recognised that analgesics, particularly opioids, can causes a reduction in the emotional distress of the pain whilst the patient experiences little to no change in the actual intensity of the pain sensation (Ribeiro et al., 2005). This is one reason why there is poor forward translation for analgesic drugs from preclinical animal studies to clinical trials as primarily only the antinociceptive drug activity is assessed preclinically whilst randomised control trials focus on endpoints relating to verbal self-reporting (visual analogue scales (VAS)) of spontaneous pain intensity reduction. To bridge the gap between promising treatments in pre-clinical animal studies and human clinical trials, primary neuropathic pain assessment endpoints need to be aligned and ideally objective biomarkers of NP.

1.5 Animal models of neuropathic pain

Animal models are extensively used to study pain, most commonly in rats and mice, as pain studies in humans are difficult to undertake as they are severely limited by ethical considerations and are often subjective (Mogil, 2009). Therefore, animal models of neuropathic pain are essential in understanding the underlying mechanisms and development of effective treatments. Effective models should create reproducible sensory deficits experienced in humans, such as allodynia, hyperalgesia, and spontaneous pain over a period of time (chronic). This should make it viable to model the pathophysiological changes observed in humans. Due to the diverse etiology and manifestation of neuropathic pain, a large range of animal models are used, including the sciatic constriction injury (SCI)-induced peripheral and central pain model, chemotherapy drug induced, diabetes induced, human immunodeficiency virus (HIV)-induced, trigeminal neuralgia, and orofacial pain models. Due to the high prevalence of diabetes, animal models of diabetes and associated complications are of particular value. For example, streptozotocin-induced diabetic rats (STZ) and diet induced diabetic models. STZ is a naturally occurring chemical derived from *Streptomyces achromgenes.* It is taken up by pancreatic β cells through the GLUT2 transporter and causes alkylation and free radical damage of DNA, leading to cell death and thus decreased insulin secretion (Lenzen, 2008). A one-time injection either intravenously or intraperitoneally induces type 1 diabetes in rodents and produces pain phenotype in around 80% of animals which exhibit thermal hyperalgesia, hypoalgesia and mechanical allodynia; this pain phenotype is higher than that exhibited in patients which is around 30% (Field et al., 1999; Abbott et al., 2011). STZ induced diabetic animal models have been widely studied to investigate underlying mechanisms behind these abnormal sensations and pain responses. In diet induced diabetic animal models, animals are fed a high fat/high glucose diet which causes obesity and leads to type 2 diabetes (Surwit et al., 1988). This is a useful model due to the rising prevalence of obesity and type 2 diabetes in humans, with over 6% of the world's population having type 2 diabetes, a figure which is predicted to increase to over 7% by 2030 (Khan et al., 2020). In addition to this neuropathy often manifests in patients before they are diagnosed with diabetes, so it's hoped that a diet induces type 2 animal

model could provide insight into the progression and prevention of nerve dysfunction in these patients (Stino & Smith, 2017).

Although rodents are commonly used in preclinical pain animal studies, pain and analgesia cannot be verbally self-reported and can only be inferred from observations made by hunas which present a challenge in rodents (Percie du Sert & Rice, 2014). Further, as pain is an unpleasant sensory and emotional experience reflexive sensory reaction to stimuli does not necessarily mean it is a painful experience (Sandkuhler, 2009). Many research groups are now looking to improve the markers used preclinically and clinically with the goal of producing biomarkers that can successfully forward translate preclinical candidates to human clinical trials.

1.6 Biomarkers

Biomarkers are characteristics that can be objectively measured and used as an indicator of biological processes (Biomarkers Definitions Working Group, 2001). In relation to pain, biomarkers would be able to objectively indicate the intensity and development of the pain, as well as provide information so the optimal treatment can be given to that particular patient. In neuropathic pain it is problematic to decipher between specific pain mediators and pathophysiological changes where pain is just a symptom. For this reason, measuring and evaluating changes and patterns in a range of small molecules and peptides found peripherally would be a good indicator to the severity and development of the neuropathic pain. Changes in intraepidermal nerve fibres and levels of several molecules in the periphery have been identified in preclinical animal pain models and in patients which could potentially translational biomarkers.

Although the assessment and identification of biomarkers for neuropathic pain are essential to bridge the gap between promising treatments in pre-clinical animal studies and human clinical trials, as well as monitoring the progression of the neuropathic pain and individualising therapeutic treatment, they are not without their limitations. One issue is that the concentration of the biomarkers may fluctuate drastically in animal subjects as well as in human patients. This is a consequence of physiological adaptations because of pain, biological variability, comorbidities, and changes to metabolic processes due to age and pharmacological treatment. A further issue is that although a biomarker may be able to predict the severity of the neuropathic pain and its progression its assessment may only be accurate and reliable for a set period of time in the disease progression. As the biomarkers themselves may change during the progression of the disease, as well as possibly through different time points in the day and between genders.

1.7 Intra Epidermal nerve fibres (IENFs)

Skin biopsies are a valuable diagnostic tool for peripheral neuropathies as it allows for the assessment of small unmyelinated fibres that are usually hard to evaluate. Intra-epidermal nerve fibres (IENF) are predominantly capsaicin sensitive unmyelinated c-fibres which detect thermal nociceptive pain (Nolano et al., 1999, Figure 1). Small sensory C-fibres emanate from the DRG and as they cross through the epidermal-dermal border into the epidermis they become de-myelinated, losing their Schwann cell ensheathment, terminating as free nerve endings lacking structure (Wang et al., 1990). They can broadly be categorised into two groups, peptidergic and non peptidergic. Peptidergic fibres express proteins such as cGRP and substance P and are responsive to nerve growth factor as they exhibit their receptor tropomyosin receptor kinase A (Trka) (Snider and

McMahon,1998). Quantification of epidermal nerve fibres can be used to detect neuropathies at different stages of progression/development as well as evaluation of therapeutic treatments.

This is especially useful in DPN as the hands and feet are often affected, and it has been deduced that there is dysfunction to epidermal c-fibres which respond to stimuli (Polydefkis, Griffin, & McArthur, 2003). IENF density is reduced in those with diabetic neuropathy, and a change can be seen before painful symptoms are generated (Kennedy, Wendelschafer-Crabb & Johnson, 1996). The decrease in density declines as the severity of the neuropathy increases, which aligns with the expected pathology of diabetic neuropathy (Arimura et al., 2013). With age there is a decline in IENF density in healthy individuals, however this is expedited in diabetics and there is a greater rate of decline (Narayanaswamy et al., 2012). In addition to this, IENF density in diabetics correlates with thermal thresholds, pressure sense and total neurological disability score, meaning it is a reliable means of evaluating diabetic neuropathy (Pittenger et al., 2004; Shun et al., 2004). Due to small sensory IENF mediating nociception, it is plausible that there is a greater decrease in IENF density in painful neuropathies compared to painless, however research has thus far established that this is not the case. In a large cohort study between people with painless and painful diabetic neuropathy, no difference was found between IENF density even though those experiencing neuropathic pain had more serve neuropathy (the Toronto Clinical Scoring System was used as a screening tool for diabetic neuropathy and correlates with diabetic neuropathy severity) (Themistocleous et al., 2016). In this study protein gene product (PGP) 9.5 was used to quantify IENF density, suggesting that PGP 9.5 quantification is unable to decipher between painful and painless diabetic neuropathies.

Antibodies against neuronal marker proteins allow for assessment of IENFs. PGP 9.5 is commonly used which is a highly conserved cytosolic ubiquitin carboxyl terminal hydroxylase found in all neurones, anti-PGP 9.5 antibodies binds to both peptidergic and non-peptidergic epidermal nerve profiles, therefore can be used as a neuronal marker (Dalsgaardet al., 1989). These have been used extensively to mark intraepidermal nerve fibres in humans with diabetic neuropathy and in animal models of diabetes. In human skin biopsies, it has been shown there is a reduced immunoreactivity to PGP 9.5 (Levy et al., 1989). This reduction in IENF density using anti PGP 9.5 antibodies has been confirmed numerous times in subsequent studies showing that it is a reliable marker (Gibran et al., 2002; Pittenger et al., 2004; Shun et al., 2004; Koskinen et al., 2005*).* Additionally, animal models type of type 2 diabetes have also shown a reduction in IENF density compared to control animals using anti PGP 9.5 antibodies (Andreasen et al., 2020). However, the apparent lack of discrimination PGP 9.5 offers between painful and painless neuropathies indicates that other molecular markers of IENF or assessment of morphological characteristics are needed.

Figures 3 and 4 depict an illustration of IENF staining with primary antibody PGP 9.5 IHC in a skin biopsy from a rat model of diabetes (Figure 3) and in a human skin biopsy (Figure 4). Both figures, show a similar pattern of decreasing nerve fibre length and density between control tissue and diabetic tissue. Showing that IENF characteristic assessment translates well between animal models and humans.

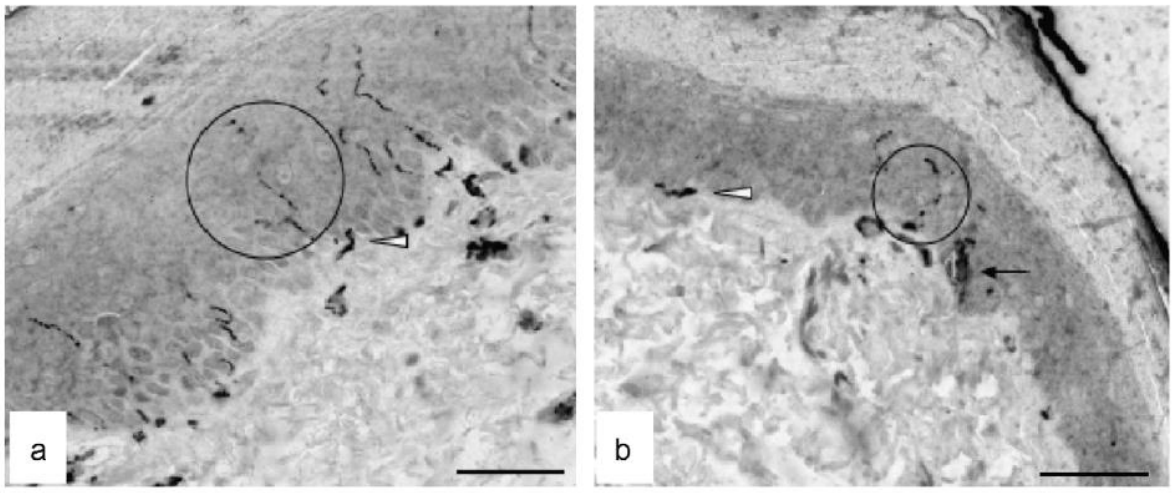

Figure 3. plantar skin from a control rat (a), and a STZ-injected rat that developed diabetes and neuropathy (b) (Beiswenger et al., 2008). The circles show the IENF labelled with the neuronal marker PGP 9.5. There is a decrease in length and density of never fibers in the diabetic tissue compared to the control, the axons also become noticeably swollen in the diabetic tissue, shown by the back arrow. White arrows in in (a) and (b) indicate dermal nerve fibre bundles. The scale bar is 50um.

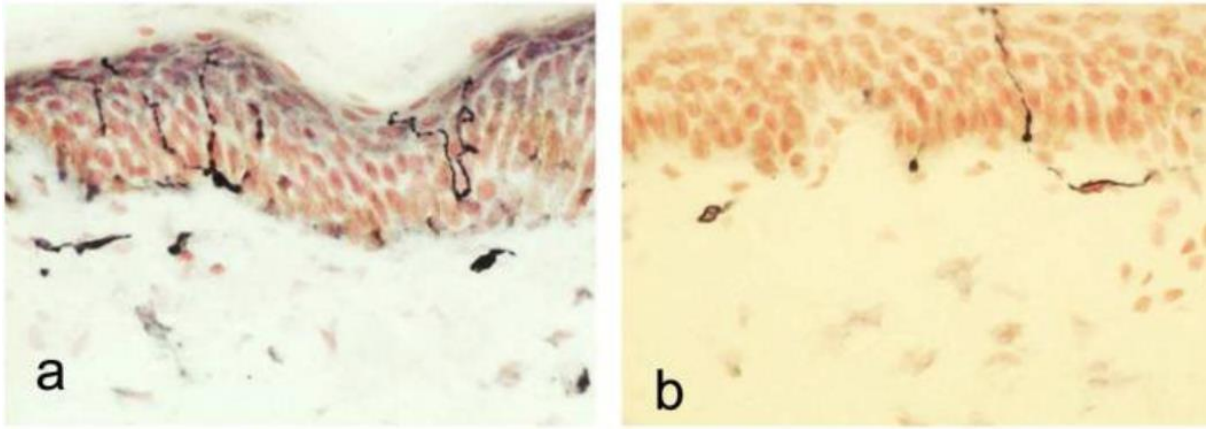

Figure 4. PGP 9.5 immunoreactivity in calfskin: healthy (a), painful diabetic neuropathy (b) (Shillo et al., 2021). Immunostaining shows a reduction in the amount of IENFs between the healthy cand diabetic calfskin.

Along with quantifying IENF density, examining the morphological characteristics of IENFs can be used as a biomarker of peripheral neuropathy. This includes evaluating the structural features of the nerve fibres such as their length, amount of branching, branching pattern and axonal diameter (presence of axonal swelling) (Wendelschafer-Crabb, Kennedy & Walk, 2006). A 2007 study in diabetic patients with painful neuropathy found a decrease in IENF length but observed no changes in IENF density or the amount of axonal branching (Quattrini et al., 2007). However, in a 2017 study comparing painless and painful diabetic neuropathies there was no observed difference in IENF length between the two groups (Bönhof et al., 2017). Along with epidermal and dermal nerve fibre length, another characteristic of IENFs found in peripheral neuropathies is axonal swelling, in which axons have twice the diameter of the parent fibre. Although the consequence of this swelling is unknown it is believed that it influences signal propagation and is perceived to mark a decline in

epidermal innervation, conversely not only may this be a marker of neuronal degeneration but also a marker of neuronal regeneration (Wendelschafer-Crabb, Kennedy & Walk, 2006). For this reason, although it was thought that there may be a difference in the amount of axonal swelling observed between painful and painless neuropathies, this relationship has yet to be found. As in a 2015 study there was found to be no correlation between pain and axonal swelling (Cheung et al., 2015). However, in this same study it was shown that axonal swellings show immunoreactivity to TrkA and substance P, which are known nociceptive pain markers, therefore may be a marker for neuropathic

1.8 Langerhans cells (LCs)

Langerhans cells (LCs) are the resident macrophages in the epidermis of the skin, where their primary function is antigen recognition and presentation. They are dendritic cells with a stellate shaped appearance. There is a close association between LCs and nerve fibres in the epidermis, as it has been found that LCs synthesise neuromodulators such as cGRP and substance P (Hosoi et al., 1993). Suggesting that LCs and small nerve fibres in the epidermis may be integrated in a neuro-immuno-cutaneous system (Misery, 1998). LCs also produce PGP 9.5 when they are denervated (Hsieh et al., 1996). Meaning they can be visualised using an anti PGP 9.5 antibody. Their role in neuropathic pain has been studied in rodent models as well as in humans. There has found to be an increase in PGP 9.5 immunoreactive LCs in rodent models of sciatic nerve constriction, and crush or chronic constriction of the sciatic nerve (Hsieh et al., 1996; Lindenlaub & Sommer, 2002). An increase in LCs has also been displayed in humans with complex pain regional syndrome (Calder, Holten, & McAllister, 1998). In a 2012 study investigating distal small fibre neuropathy in diabetic patients with neuropathic pain (n=13), non-diabetic patients with (n=7) and without (n=6) neuropathic pain, it was found that diabetes was associated with an increase in the number of LCs and that there was a negative correlation between the IENFD and the number of LCs (Casanova-Molla et al., 2012). Therefore, it is speculated that LCs may play a role in the sensitisation of nociceptive terminals and in the generation and maintenance of neuropathic pain. Thereby being a good biomarker of neuropathic pain.

1.9 Calcitonin gene-related product (cGRP)

Calcitonin gene-related peptide (cGRP) causes vasodilation and neurogenic inflammation. It is implicated in pain pathways as it is released and expressed from peptidergic sensory neurons, and there is growing evidence to suggest it is involved in the development of neuropathic pain. Its role in migraine attacks has been widely studied and anti cGRP antibodies have been approved as a therapeutic treatment for migraine (Spindler & Ryan, 2020). In a 2020 study, patients who suffered from migraines and peripheral neuropathy were treated with an anti-CRGP antibody. This led to patients reporting a 40% decrease in score on the neuropathy pain scale (Kang & Govindarajan, 2021). Studies using animal models of pain have shown a correlation between neuropathic pain and elevated levels and upregulation of cGRP. When rats were subjected to a ligation on the L_5 and L_6 spinal nerves it caused hyperalgesia and allodynia (hallmarks of neuropathic pain), and there was also a marked increase in the release of cGRP (Gardell et al., 2003). In another study when rats were persistently exposed to morphine causing abdominal pain, there was an increase in the upregulation of cGRP in the spinal dorsal horn (Gardell et al., 2002). When treatment was administered to the rats to attenuate the pain, the reduction in abdominal pain was accompanied by a decrease in the elevated cGRP levels. These studies suggest that cGRP plays a role in contributing to neuropathic pain, possibly making it a good target to evaluate levels of neuropathic pain in animal models.

Peptidergic nerve fibres also express TrkA, a receptor for nerve growth factor (NGF), which regulates neuropeptide expression. NGF-Trka signalling pathway has been implicated in pain generation and maintenance, and its activity has been found to be increased in painful diabetic neuropathy (Evans et al, 2012). The study found that although IENF density was decreased in diabetic planar skin there was a proportional increase in IENFs labelled with cGRP compared to controls. However, this hasn't be shown in humans. Possibly because cGRP-immunoreactive profiles terminate in the dermis of human skin (Gibbins, Furness & Costa, 1987). But it remains possible that cGRP immunoreactivity may be able to distinguish between painful and painless neuropathies in animal models, as well as being a useful biomarker of peripheral neuropathy and neuropathic pain.

1.10 Vascular endothelial growth factor (VEGF): marker of angiogenesis

There has been observed changes in blood flow and blood flow regulation in both painful and diabetic neuropathies with differing endothelial dysfunction between the two. In patients with advanced diabetic neuropathy, it was found that an increase in blood vessels and a decreased ratio to epidermal nerve fibre density differentiated painful neuropathies from painless (Shillo et al., 2021). This could be a result of altered levels of Vascular endothelial growth factors (VEGF). As there is an evident angiogenic paradox in diabetes, as there are a number of diabetic complications associated with impaired angiogenesis (neuropathy, wound healing) but also increased angiogenesis (retinopathy) (Costa & Soares, 2013). Whilst sensory neuronal expression of VEGF decreases in STZ diabetic rats, the total VEGF plasma levels are raised in symptomatic diabetic neuropathy (Pawson et al., 2010; Deguchi et al., 2009). VEGFs are a family of angiogenic factors, derived from endothelial cells in hypoxic environments and it has been shown that VEGF levels are increased in periphery neuropathies (Collins et al., 2003). VEGFs have also been shown to be neuroprotective agents, in particular VEGF-A which has displayed neuronal protection and regeneration (Sondell, lundborg & Kanje, 1999). Therefore, it's hypothesised that VEGF could have therapeutic actions against peripheral neuropathies and could be used as a marker of neuropathic pain. Studies have shown that two splice variants of VEGF-A, VEGF-A_{165}a and VEGF-A_{165}b, are implicated in the attenuation of neuropathic pain. In a 2015 study, mice were administered with cisplatin, a chemotherapy treatment, which induced neuropathic pain displayed by a significant decrease in mechanical withdrawal threshold and a reduction in nociceptive response latencies (Vencappa, Donaldson, & Hulse 2015). It was found that expression levels of the total amount of VEGF-A isoforms was significantly decreased in the mice treated with cisplatin compared to the vehicle treated group. In the same study exogenous VEGF-A was co administered with cisplatin treatment. When either rhVEGF-A_{165}a or rhVEGF-A_{165}b was administered, along with cisplatin, they had a neuroprotective effect as they prevented the reduction in neutral length caused by the cisplatin. In another study it was shown that treatment with VEGF-A_{165}b, in STZ induced diabetic rats, was neuroprotective as it reduced elevated pain behaviour, epidermal sensory loss, and aberrant sciatic nerve morphology (Hulse, et al. 2015). These studies suggest that an alteration in VEGF-A levels could be marker for neuropathic pain.

1.11 Hind plantar skin: Glabrous skin

In many animal models behavioural tests in vivo and in vitro assessment of biomarkers for peripheral neuropathic pain are focused on the plantar surface of the hind paws of the animals. In particular the Glabrous skin in the middle of the paw. Glabrous skin is thick and hairless and comprised of the epidermis, dermis, and hypodermis (Gould, 2018). The epidermis is made of five stratified layers, the stratum corneum, lucidum, granulosum, spinosum, and basale (figure 5). The stratum corneum is the

outer most layer of the epidermis made of dead, non-nucleated keratinocytes (pink layer figure 5). Keratinocytes are the predominant cell type in the epidermis, they originate from stem cells in the basale layer and continuously migrate through the epidermis to the corneum layer and desquamate. The stratum lucidum is also made of dead cells and is a translucent layer comprised of keratein filaments (blue layer figure 5), whilst the stratum granulosum is made of flattened mature keratinocytes with lamellar granules (dark red layer figure 5). The stratum spinosum contains keratin fibrils as well as melanosomes (brown figure 5) and Langerhans cells (red and purple figure 5). Melanosomes produce and store melanin and Langerhans cells are antigen presenting macrophages. The basale layer is comprised of stem cells responsible for generating keratocytes and pushing them upwards. Below the epidermis comes the dermis, an irregular arrangement of connective tissue predominantly made of type I collagen, type III is also present as well as type IV collagen which envelops Schwann cells at the epidermal-dermal junction. It can be divided into two layers, the papillary dermis and reticular dermis. Nociceptive C fibres branch across the epidermal-dermal junction whilst the many other somatosensory neurons terminate in the dermis, these receptors include Ruffini endings, Pacinian corpuscle, Meissner corpuscle, and Merkel cells (figure 6)

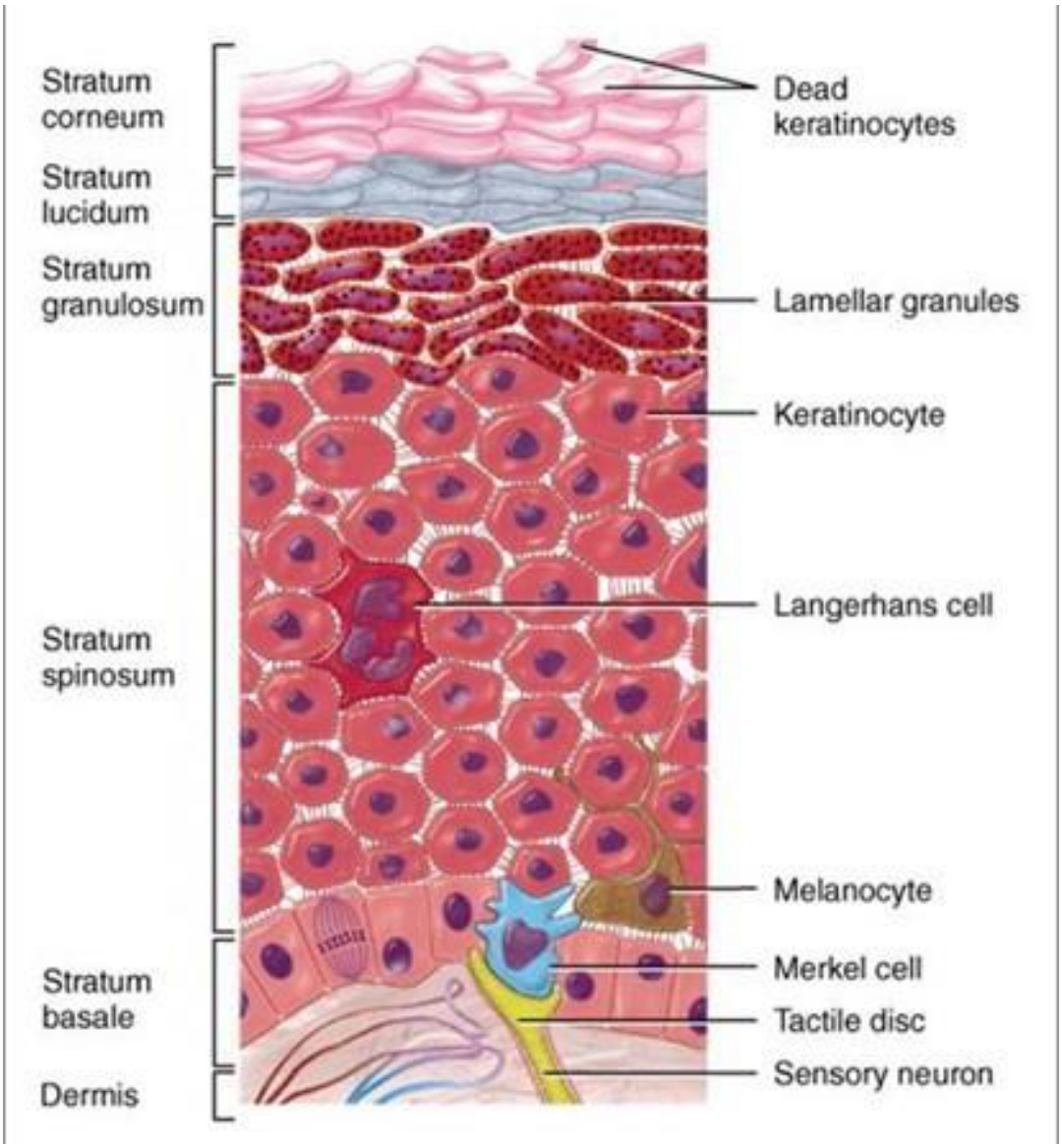

Figure 5. Layers of the epidermis in glabrous skin (Image adapted from Tortora and Grabowski, 2001). The five stratified layers of the epidermis are, the stratum corneum (pink), lucidum light blue), granulosum (dark red), spinosum (dark peach), and basale (light peach). The main cell types present are keratinocytes (peach and purple), melanocytes (brown), Langerhans cells (red), and Merkel cells (blue).

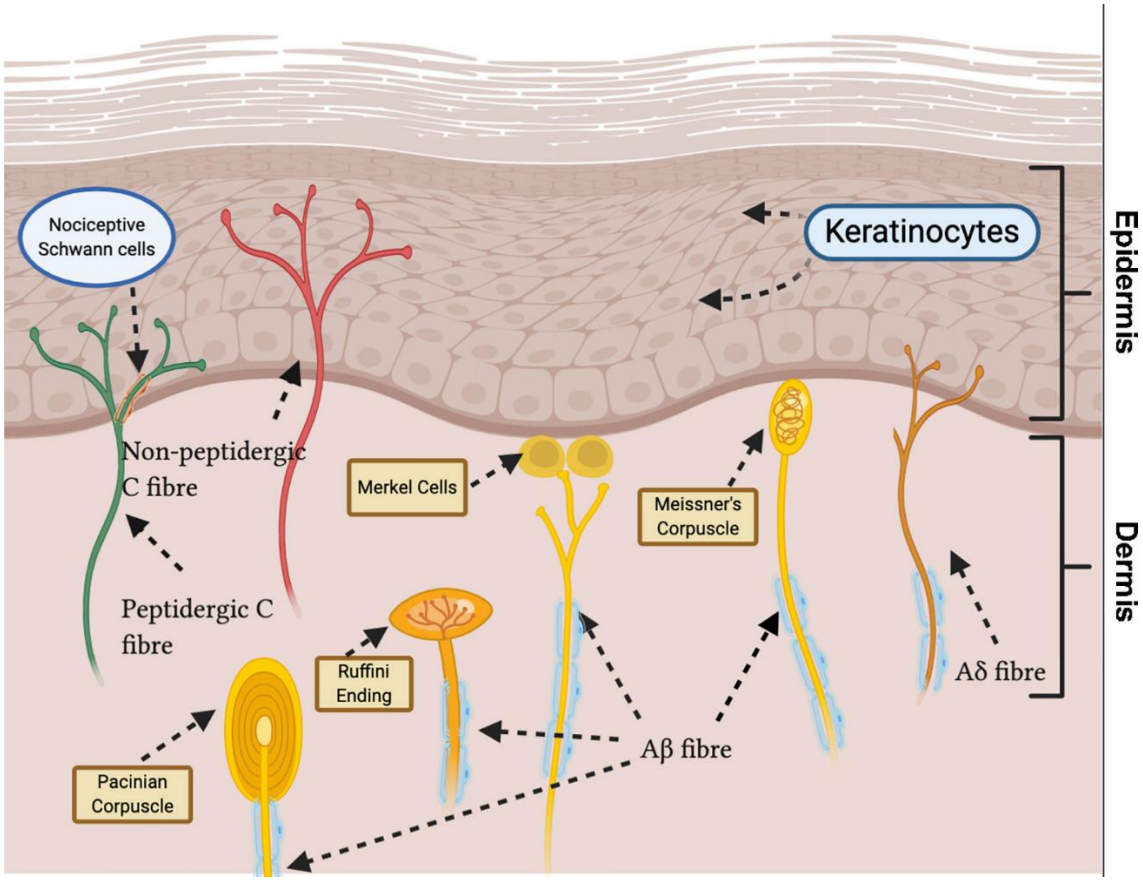

Figure 6. Sensory innervation in glabrous skin (Lowy, Makker & Moalem-Taylor, 2021). Unmyelinated C fibres (peptidergic and non-peptidergic) terminate in epidermis as free nerve endings. Aδ fibres also terminate as free nerve endings. Myelinated Aβ fibres terminate in the dermal layer as: Ruffini endings, Pacinian corpuscle, Meissner corpuscle, and Merkel cells

1.14 Project aims and objectives

Diabetic peripheral neuropathy affects more than half of all diabetic patients, with neuropathic pain being the most common symptom (Obrosova, 2009). However, the underlying pathophysiology is often heterogenous and poorly understood resulting in only a small percentage of patients benefiting from current treatments options. This is compounded by poor translatability of drugs from positive preclinical results into successful human trials. Without biomarkers that predict neuropathy and / or neuropathic pain, the optimum treatment strategy for the patient's neuropathic pain cannot easily be selected or identified preclinically for successful translation. The work in this thesis aims to characterise peripheral neuropathy and biomarkers as predictors of neuropathic pain in preclinical models of type 1 and 2 diabetes. Plantar skin biopsies from type 1 STZ-induced diabetic rats with a stable mechanical allodynia after 7 weeks and type 2 high fat diet

induced diabetic mice will be analysed in order to correlate the extent of peripheral epidermal/dermal nerve fibre damage with mechanical allodynia sensory pain phenotype.

It is hypothesised that there will be an observed decrease in the IENF density and increased intra-epidermal Langerhans cell number in type 1 and 2 diabetic animals expressing mechanical allodynia, but not in control, non-diabetic or diabetic non-pain phenotypic animals. To determine this an optimised IHC protocol for the quantification of epidermal/dermal nerve fibres and Langerhans cells using primary antibody PGP 9.5 was developed and implemented on type 1 and 2 diabetic plantar skin biopsies. It's also hypothesised that although it's expected to see an overall decrease in IENF density its predicted that there will be a proportional increase in cGRP immunoreactivity. This was addressed by implementing the optimised IHC protocol and instead using an anti cGRP antibody. As VEGF-A has displayed neuronal protection and regeneration, through western blot analysis in this study it is expected to see an increase in this marker in type 1 and 2 diabetic tissue.

2. Materials and methods

2.1 Animal experimentation

Tissues used in these experiments were collected from in vivo studies conducted at the University of Hertfordshire by Dr Lisa Lione and PhD candidate Michael Lanigan, and at Nottingham Trent University by Dr Richard Hulse and PhD candidate Lydia Hardowar.

All research procedures/experiments were performed in accordance with Animals Scientific Procedures Act 1986 & European Directive 2010/63/EU. All studies performed were approved by the University of Hertfordshire Animal Welfare and Ethics Review Body or the Nottingham Trent University, Clifton Campus; Ethical Review Process, and comply with the home office guidelines and codes of conduct. Careful consideration was given to the number of animals used and to the duration of their exposure to the neuropathic condition, to minimise the suffering and distress to the animals in line with the NC3Rs

2.1.2 STZ induced type-1 diabetes: 7-week timepoint study

30 Male Wister Han ISG rats (Charles River UK) were housed in pairs with food and water provided ad libitum. Animals were either dosed with a single injection (23G needle) of 55mg/kg Streptozotocin (n=18, dose volume 10ml/kg) or 20mM citrate buffer (pH 4.1, dose volume 10ml/kg, n=12). With the citrate buffer acting as the vehicle control group. Blood glucose levels were measured, using a GlucoRx Nexus blood glucose monitor, before STZ dosing (day -4) and at day 7, 21, 35, and 45 (terminal) post STZ/vehicle to monitor onset and progression of hyperglycaemia. Likewise, to monitor the animal's welfare bodyweight measurements were taken daily prior to STZ/vehicle dosing and daily thereafter. During the three weeks before STZ/vehicle dosing von Frey (VF) paw withdrawal threshold was assessed twice weekly and after dosing it was measured up to three times a week to determine and monitor the development of mechanical allodynia. In A VF test, animals are placed in a small cage with a mesh bottom and are allowed to acclimatise before any testing commences. Monofilaments (von Frey filaments) are placed perpendicular under the hind foot pad of the animal and applied to the plantar skin until it buckles, delivering a uniformed and constant force for a set period of time (2-8 seconds). A positive result is considered if there is immediate withdrawal or licking of the paw. Von Frey filaments come in a range of weights therefore a known predetermined force can be applied. There a several different methodologies used to conduct a von Frey test, these include the up down, ascending, and percent response method. The effect of Pregabalin (3, 10 or 20mg/kg po, daily) or vehicle dosing on this mechanical allodynia was also assessed from week 4 onwards. Burrowing habituation was evaluated before and after STZ dosing to monitor animal wellbeing and to assess the impact of pain on behaviour as an alternative objective endpoint.

Animals were sacrificed on day 45 using a schedule 1 method of rising concentration $C0_2$, following confirmation of death, plantar skin from both hind paws were harvested. Paw skin samples were placed and stored in 4%PFA (10% neutral buffered formalin). Right paw pads were subsequently removed from the PFA after 24hrs, rinsed in PBS and placed in 30% sucrose solution before being frozen flat in tinfoil with a few drops of OCT. These cryoprotected tissues were then stored in a freezer at -80°C.

2.1.3 STZ induced type-1 diabetes: 2- and 4-week timepoint study

A separate study following a similar protocol as the 7-week STZ study (2.1.2) was completed. A smaller cohort of 16 Male Wister Han ISG rats (Charles River UK) were housed in pairs with food and water provided ad libitum. Animals were either dosed with 55mg/kg Streptozotocin (n=12) or 20mM citrate buffer (pH 4.1, n=4). Bodyweight and blood glucose levels were monitored before and after STZ/vehicle dosing to assess the onset and progression of hyperglycaemia as well as to monitor the welfare of the animals. Mechanical allodynia was assessed using von Frey paw withdrawal threshold, which was measured on three occasions before dosing and four times afterwards. Animals were sacrificed using the same schedule 1 method as 2.1.2 on day 14 (control n=2, STZ n=6) and day 28 (control n=2, STZ n=6). Plantar skin from both hind paws were harvested and placed and stored in 4%PFA (10% neutral buffered formalin). Retinas from both eyes were also collected from the animals sacrificed at 4 weeks. Individually the retinas were removed and ground in liquid nitrogen. The powder was transferred into radioimmunoprecipitation assay buffer (RIPA buffer) (10ul/ml), incubated on ice for 40 minutes, with the solution being vortexed every 4-6 minuets during incubation. These were then transferred to ultra-speed centrifuge tube and spun at 10000g for 20 minutes at 4°C. the supernatant was collected and stored in freezer at -80°C.

2.1.4 High fat diet (HFD) induced type-2 diabetes mouse model: Nottingham Trent university

9 male and 9 female C57 BI6 mice (Charles River UK) where housed three in a cage with food and water provide ad libitum and allowed to acclimatise for 7 days. Animals were divided equally into 6 groups and given the treatment schedule as described in table 1.

Table 1: Treatment groups in HFD induced type -2 diabetes mouse study

Group Number	Number of Animals	Treatment
1	3	Male mice fed normal chow diet
2	3	Female mice fed normal chow diet
3	3	Male mice fed 42% fat diet following baseline measures
4	3	Female mice fed 42% high fat diet following baseline measures
5	3	Male mice fed 60% high fat diet following baseline measures
6	3	Female mice fed 60% fat diet following baseline measures

General observations and bodyweight were recorded pre/post diet intervention once a week along with blood glucose levels. This was to monitor animal welfare as well as onset and maintenance of

hyperglycaemia. Behavioural assessment of pain was evaluated using von Frey hairs and Hargreaves test. Hargreaves test is designed to assess the response to thermal pain in rodents. It utilises an optic fibre placed under the rodent's paw, which emits infrared waves to produce heat and automatically switches of when the animal withdraws their paw. Along with VF test these were conducted twice before diet intervention and once a week afterwards until the conclusion of the study. After diet intervention the study ran for 12 weeks. On completion of the study animals were killed by cervical dislocation and the death was confirmed by exsanguination. Tissues were harvested, including hind paw skin, which were placed in 4%PFA (10% neutral buffered formalin), removed after 24hrs, rinsed in PBS and placed in 30% sucrose solution before being frozen flat in tinfoil with a few drops of OCT. These cryoprotected tissues were stored at -80°C and subsequently transferred from Nottingham Trent University to University of Hertfordshire in dry ice, and again were stored at -80°C until tissue preparation and processing.

2.2 Tissue preparation: paraffin embedding and sectioning

Fixation is done to inhibit post-mortem autolysis and enzyme activity preserving the cell structures and prevents antigen diffusion; it also prevents the cells in the tissue from shrinking or swelling. Formalin is widely used as it maintains cross linking between tissues. Tissue samples stored and fixed in 10% neutral buffer formalin were removed and rinsed in PBS. Using a pair of scissors, the tissues were marked so that they could be easily identified at the end of the process. They were then placed and moved through a series of Coplin jars filled with 70, 90 and 100% ethanol for 1hr each to dehydrate the tissue. Thereby removing any water from the tissue and hardening the tissue. Samples were dried with paper between steps to limit contamination of each ethanol concentration. After the 100% ethanol tissues were placed in xylene and left overnight to clear the tissue. Due to alcohol being immiscible with paraffin the tissue has be transparentised in xylene, allowing the paraffin to absorb into the tissue. Samples were then put inside labelled cassettes and positioned in a saucepan filled with melted paraffin for 4 hrs at a temperature between 58-68°C. Metal embedding moulds along with tweezers were preheated and a tray of ice was prepared. One at a time samples were removed from the paraffin and moved into an embedding mould. Paraffin was poured into the mould and using the tweezers the tissue sample was orientated in the desired direction before moving the mould onto the ice to cool rapidly. The tissue samples were orientated so that longitudinal sections along the length of the sample could be taken. Once the wax had just began to set a cassette was placed on top of the mould and filled with wax. These were left to fully solidify on the ice before the metal mould was removed. The embedded samples could then be stored at room temperature.

Using a microtome (HistoCore biocut R) 10um sections were taken from the paraffin blocks and mounted on Epredia™ Polysine Adhesion Slides. Mounted tissue sections were left to dry at room temperature for a minimum of 24hrs before IHC staining.

Cryoprotected tissues were removed from -80°C freezer and using scissors were bisected longitudinally to give two halves of the paw skin. A few drops of OCT were placed on a cryostat mount, the tissue section was then positioned on top and covered with excess OCT. The mounted section was placed in the cryostat at -23°C and allowed to fully freeze (roughly 10 minutes). Using the cryostat (Leica CM1860 UV) 10um sections were taken from the samples and mounted on Epredia™ SuperFrost Plus™ Adhesion slides. Mounted tissue sections were left to dry at room temperature for 30 mins before being transferred to a slide box and stored in a freezer at -20°C. Before IHC staining, slides were removed from the freezer and allowed to thaw out for 30 mins.

2.3 Immunohistochemistry: PGP 9.5 and cGRP

Immunohistochemistry was performed to evaluate the density of intraepidermal never fibres and Langerhans cells. The protocol for the formalin-fixed paraffin-embedded (FFPE) tissue sections and for the cryoprotected sections are the same except for the fact the paraffin embedded sections required two additional steps prior to primary antibody incubation. As FFPE tissue sections must be deparaffinised and rehydrated, otherwise the target antigens will be obscured and won't allow for antibody binding. Slides mounted with paraffin embedded tissue were placed into histology staining boxes with horizontal slide holders. They were then run through the following solutions to deparaffinize and rehydrate the tissue sections: xylene, 100% ethanol, 90% ethanol, and 70% ethanol for 10 minutes each. Slides were then washed and left in TBS plus 0.025% triton x-100 for 5mins. Slides then underwent heat induced epitope retrieval (antigen retrieval) to break methylene bridges caused by the formalin fixation and expose the epitope. Slides were placed into vertical slide containers filled to the label of the slides with antigen retrieval solution (2.94g trisodium citrate dihydrate, 1L distilled water, 0.5ml tween 20, adjust to pH 6.0 with hydrochloric acid). Slide containers were then placed in pressure cooker, with 500ml of distilled water in the main container, and run at 110°C for 3 minutes, ensuring the lid was securely tightened. After antigen retrieval the slide holders were removed and placed in a slurry of ice and water to cool down.

Following on from antigen retrieval both FFPE sections and cryoprotected sections were treated the same. As this method relies on biotin and its binding protein streptavidin, along with horseradish peroxidase (HRP) for enzyme-mediated detection, endogenous forms of these proteins must be blocked to prevent background staining and false positive detection. This is done through the application of specific protein blocks to the tissue sections on the slides. To further reduce background staining, protein blocks and normal serum buffer are also added to the tissue section, preventing non-specific binding that primary or secondary antibodies may bind to. After this is done staining with the primary and secondary antibodies can begin.

Slides were washed with gentle agitation 2x5mins in TBS plus 0.025% triton x-100. Afterwards slides were removed, allowed to drain and dabbed on top and bottom to remove any excess liquid, and laid onto paper towel before drawing around tissue samples with a PAP pen. 2 drops of 0.3% hydrogen peroxide were added to each tissue sample and incubated for 10 minutes to block endogenous peroxidases within the sample. Excess solution was tapped of and again washed with gentle agitation 2x5mins in TBS plus 0.025% triton x-100, before being removed and allowed to drain on paper towels. 2 drops of protein block were added to the tissue sections and incubated for 10mins, afterwards excess was shaken off (important not to rinse slides). Primary antibodies against PGP 9.5 (Abcam, Cambridge, UK, ab108986, 1:300 diluted with TBS + 0.025% triton x-100) and cGRP (Abcam, Cambridge, UK, ab47027, 1:400 diluted with TBS + 0.025% triton x-100) were added to the tissue samples. Antibody dilution was determined using manufacture recommendation, available literature, and through optimisation steps described in section 2.7 (Andreasen et al., 2020) Slides were incubated in a 4°C fridge overnight (or up to 40hr) in a humid chamber (plastic takeaway box with wet paper towel at bottom and tin foil rolls to keep slides off of the paper). The next day excess primary antibody was shaken off and slides washed in TBS + 0.025% triton x-100 for 2x5mins. Biotinylated goat anti polyvalent was added to the slides and incubated in the humid chamber at room temperature for 1hr. Afterwards they were washed in TBS + 0.025% triton x-100 for 2x5mins, before being incubated with streptavidin peroxidase for 10mins and being washed again for 2x5 mins in TBS + 0.025% triton x-100. 30ul of DAB chromogen was added to 1.5ml DAB substrate in a 5ml dropper bottle. DAB substrate reacts to the HRP and forms a coloured insoluble precipitate at

the antigen location. This DAB solution was then incubated with the tissue samples for 5 minutes or until colour change was observed (which ever one came first), and then immediately washed in TBS + 0.025% triton x-100 for 5 minutes. Slides were then dehydrated in 70%, 90%, and 100% ethanol for 10 minutes each before being placed in xylene. Slides were removed individually from the xylene and a cover slip was mounted using 2 drops of DPX mountant. Mounted slides were stored indefinitely at room temperature and visualised under a light microscope. The hydrogen peroxide, protein block, biotinylated goat anti polyvalent, streptavidin peroxidase, and DAB used were from the Abcam Rabbit specific HRP/DAB (ABC) Detection IHC Kit (ab64261).

2.4 Quantification of IENFD and LCDs

Slides were visualised under a brightfield microscope at 40x magnification and pictures were captured using a camera (Nikon eclipse TE2000-U) The images were imported into Image J (Rasband, W.S., ImageJ, U. S. National Institutes of Health, Bethesda, Maryland, USA, https://imagej.nih.gov/ij/, 1997-2018) so measurements could be made. Three stained slices (triplicate) from each animal were analysed. The number of nerve fibres and Langerhans cells were counted in 5 different areas of each section (totalling 15 measurements from each animal). The length of the epidermis at the boundary to the stratum corneum at each area was measured so that the linear density of the IENFs and LCs could be calculated. Strict counting rules were applied to accurately record the number of fibres crossing the epidermal-dermal boundary as well as isolated nerves in the epidermis that do not cross the intersection. An outline of the rules with examples is given in figure 7. To help avoid bias and add blinding the label identifying the tissue type on the slide was covered by opaque masking tape and assigned a random number. Once all the slides had been visualised and quantification had taken place the masking tape was removed, and data was labelled with the correct tissue information.

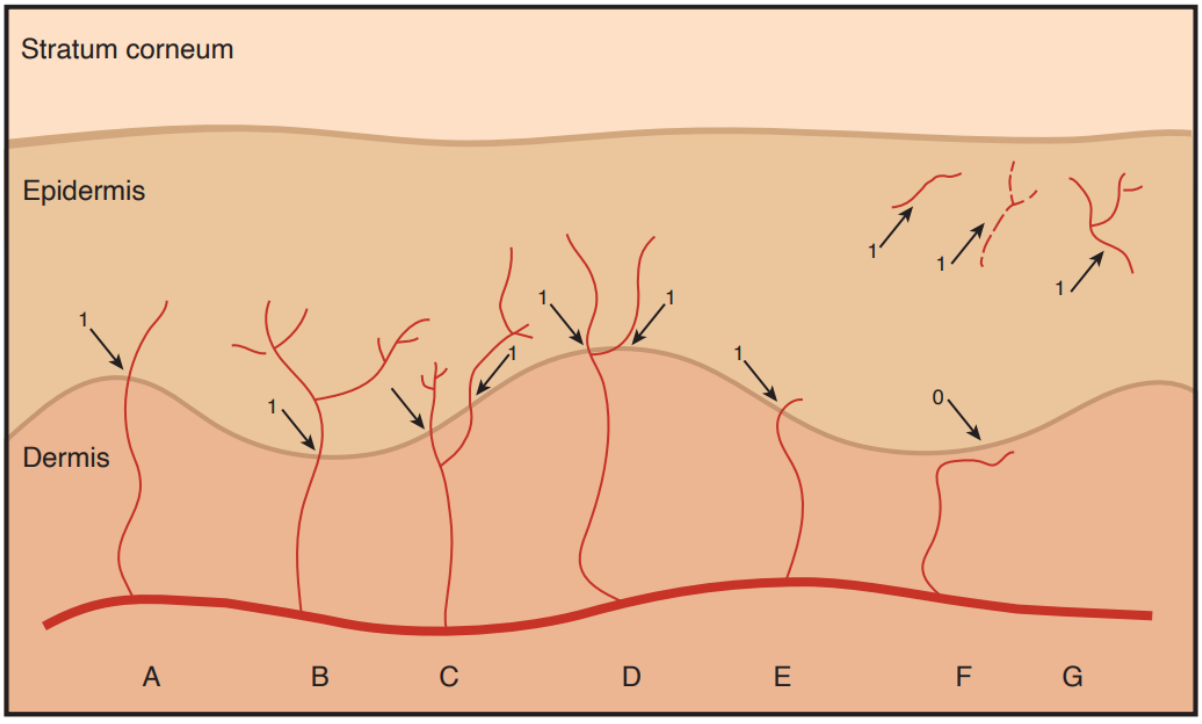

Figure 7. Nerve fibres are shown in red; the epidermis is beige, and the dermis is light red. Counting rule, A) nerves are counted as they cross the basement membrane off the epidermis. B) Nerves are counted a single unit when they branch after the basement membrane. C) Nerves are counted as separate entities when they branch below the basement membrane. D) Nerve fibres which appear

to branch in the basement membrane or it its ambiguous are counted as separate units. E) Any nerve fragments which cross the basement membrane are counted. F) nerve fibres that do not cross the membrane are not counted. G) Nerve fibre profiles and fragments which are only present in the epidermis and do not cross the basement membrane are counted.

2.5 Protein levels of VEGF: western blot

Total protein concentration from the supernatant collected form the retina tissue was calculated by the Bicinchoninic Acid (BCA) assay using Bio-Rad Protein Assay Dye Reagent. 20ug of protein from each lysate was boiled at 95°C for 15 minutes with 4x Laemmli buffer supplemented with 10% β-mercaptoethanol. The samples were then loaded into 10% Mini-PROTEAN TGX Precast gels, 12-well (Bio-Rad), along with Bio-Rad Precision Plus Protein Dual Colour Standards protein ladder to act as a reference sample to calculate protein weight during western blotting. Gel electrophoresis was conducted, to separate the proteins, using Bio-Rad Vertical Electrophoresis Cell systems at 180V filled with running buffer until gel was fully resolved (around 50 minutes). The gel was then rinsed in transfer buffer before assembling the transfer sandwich in Bio-Rad cassette: 2x foam pad, filter paper, gel, nitrocellulose membrane, filter paper, 2x foam pad. Making sure that the gel was on the anode side and the blot on the cathode. Air bubbles were removed using a roller and the cassette was placed in the transfer tank and ran at 19v for 36 minutes. The resulting nitrocellulose membrane was rinsed with 5% milk-TBST and then blocked with 5% milk-TBST on a horizontal rocker for 2hrs. Primary antibody VEGF-A (Sigma-Aldrich, Gillingham, UK, abs82, 1:1000 diluted with 5% milk-TBST) was incubated overnight on a horizontal shaker at 4°C. The blot was rinsed 3x 5 mins with TBST, before being incubated with species specific HRP-conjugated secondary antibody (Sigma-Aldrich, Gillingham, UK, 12-348, 1:5000 diluted with 5% milk-TBST) for 1hr at room temperature on horizontal rocker. The blot was rinsed 3x 5 mins with TBST and Thermo Scientific™ SuperSignal™ West Pico PLUS chemiluminescent substrate was added to the blot according to the manufacture's recommendations. The chemiluminescent signals were captured using (Thermo scientific myECL imager) and the imageJ was used to read the band intensity of the target proteins. The blot was then rinsed under running water and washed 5x 5mins in TBST, before being blocked in 5% milk-TBST on a horizontal rocker for 2hrs. The primary antibody step and onwards was then repeated using GAPDH (Proteintech, 10494-1-AP, 1:5000 diluted with 5% milk-TBST) as a loading control. The loading control protein levels were used to normalise the target protein levels.

2.6 Statistical analyses

Results are presented as mean ± SEM and were statically analysed and visualised in Graph-Pad Prism® (GraphPad Software Inc., 9.0 for Windows, SanDiego, CA, USA). Group means were compared using independent samples t-test, one-way analysis of variance (ANOVA) or multiple comparison two-way ANOVA. Associations with nerve parameters and pain phenotype data were determined by Pearson correlation. Values of $p < 0.05$ were considered statistically significant.

2.7 IHC protocol optimisation and confirmation of antibody selectivity

Although IHC is a well-established technique it isn't without its disadvantages and limitations. The procedures and stains used aren't standardised and it can be hard to decipher what the best stains to use are. In addition, well-trained personnel with a high skill base are needed to eliminate human error. Due to the subjective nature of interpreting visual images, it can also be challenging to

quantify results. To overcome these problems protocol optimisation steps were taken to develop high quality staining and robust quantification methods.

The first issue encountered was tissue sections not adhering to the slide properly and becoming displaced (folding or falling off) during washing steps in the protocol (Figure 8). Different buffers were used see if this had an impact however it was found that changing the slide type fixed the problem. For formalin-fixed paraffin-embedded tissue Polysine adhesion slides, which are electrostatically and biochemically adhesive, were used. And for cryoprotected tissue SuperFrost plus adhesion slides worked best. Changing the slide type mitigated the tissue falling off during washes however during antigen retrieval in the pressure cooker tissues would often be displaced from the slides. Two things were changed to fix this. Firstly, the antigen retrieval solution was adjusted to be at the correct pH (pH 6), and secondly the pressure cooker was operated at a higher temperature for a shorter amount of time. Multiple runs with different combinations of time and temperature were completed to establish what produced the best results. It was essential for FFPE tissue sections to be put through antigen retrieval otherwise no staining would occur in the tissue.

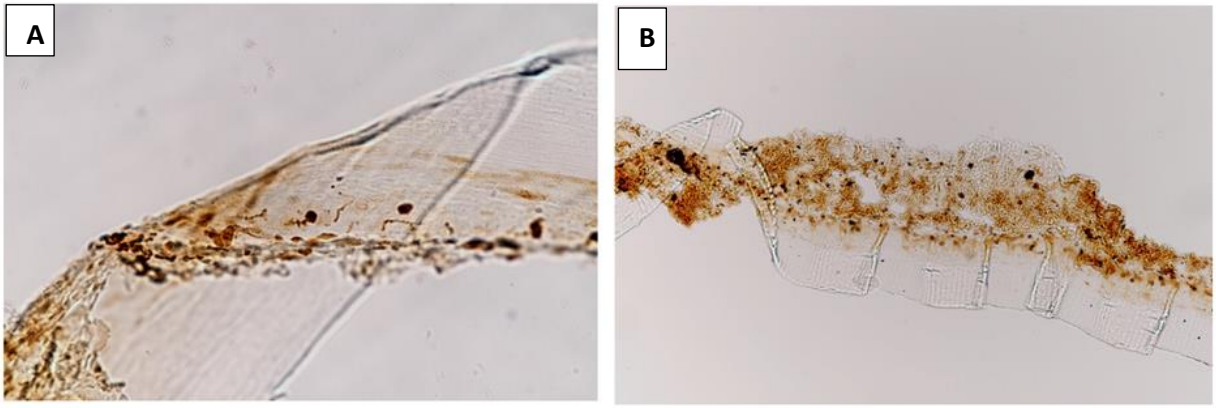

Figure 8. Folding (A) and creasing (B) of tissue sections mounted on slide due to poor adhesion and improper antigen retrieval procedure. Control rat tissue sections stained with PGP 9.5.

A similar procedure was adopted to work out the optimal dilution factor for the primary antibody. Dilutions of 1:100, 1:200, 1:300, 1:500, and 1:1000 were tested, these dilutions were based on typical primary antibody concentrations for IHC. Along with this three different dilutants were used to see if this had any effect. The diluents had little to no effect, so TBS+ 0.01% triton x-100 was used as this was readily available. For both PGP 9.5 and cGRP an antibody dilution of 1:300 produced optimal level of staining (figure 9). Below this dilution there was over staining, and it became hard to decipher the individual fibres, whilst dilutions above 1:300 developed very little staining (figure 10). Another contributor to the level of staining was how long the tissue sections were incubated with DAB towards the end of the protocol. The correct duration of time was determined by allowing the tissue sections to change colour then taking one slide every 10 seconds washing off the DAB reagent and then using a microscope to establish the optimal level of staining. Although the sections changed colour quickly (less than 30 seconds), the best results were found by leaving the stain to develop on the sections for 3 minutes.

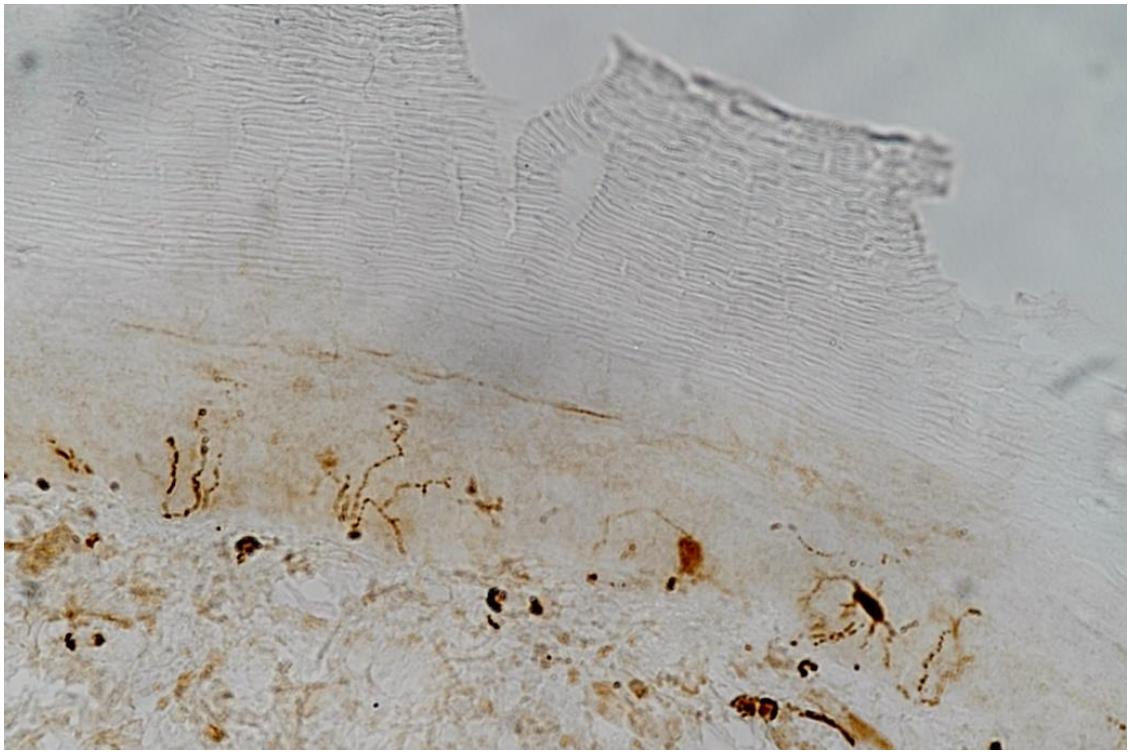

Figure 9. Optimal level of staining with PGP 9.5 to quantify IENFs and Langerhans cells. Normal innervation of healthy rat plantar skin at 40x magnification.

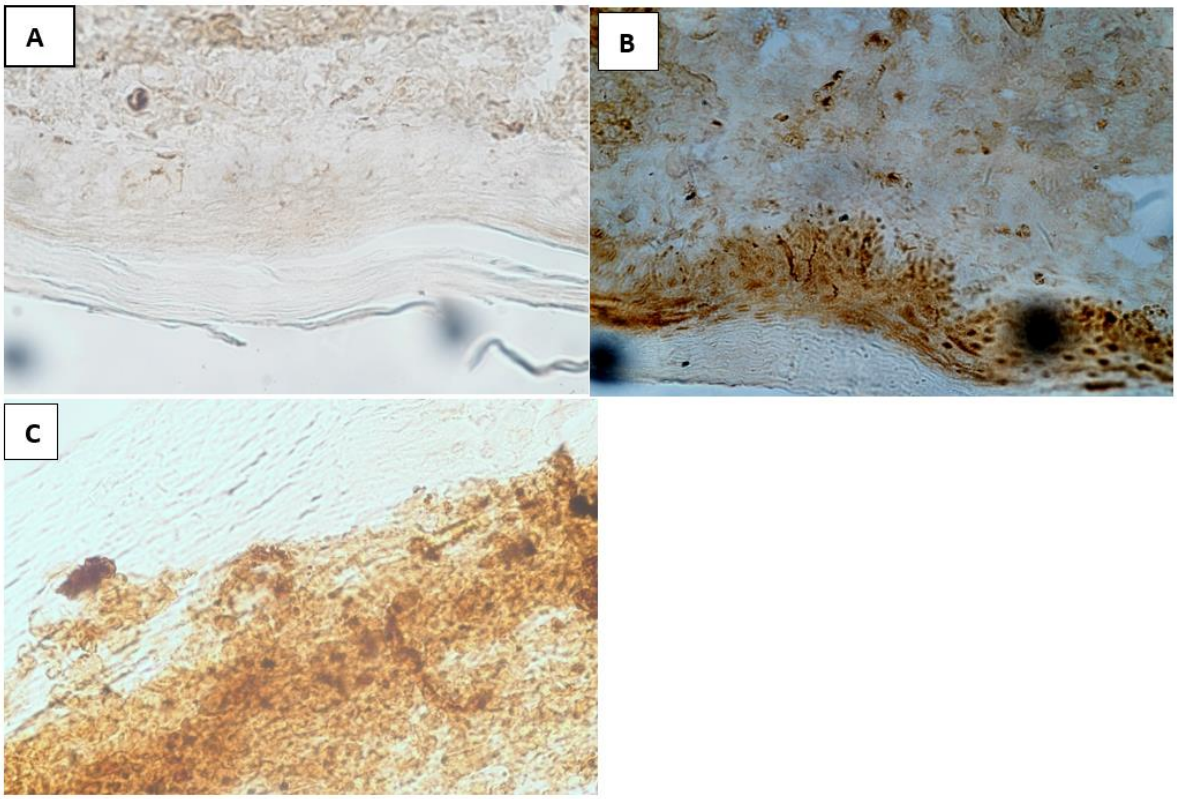

Figure 10. examples of over/under staining of IENFs with PGP 9.5, in control rat plantar skin tissue ate 40x magnification. (A) Under-staining caused by the antibody being to dilute. (B) Over-staining

caused by to concentrated antibody. (C) Over-staining because of too long incubation with DAB chromogen.

Throughout these optimisation steps different section thicknesses were also being tested, ranging from 5um-30um. 10um sections were deemed the most appropriate for several reasons. They produced repeatable slices which sliced well and adhered to the slide strongly, and during sectioning they didn't become compressed. They also produced stained samples that were easy to visualise and analyse under a brightfield microscope. Along with section thickness the correct orientation for sections to be taken from the tissue had to be determined. IENFs were best visualised when longitudinal sections were taken compared to transverse. Confirmation of antibody selectivity was determined by running staining protocol with either no primary antibody or no secondary antibody. When not used in conjunction no staining was present.

3. Results

3.1 STZ induced type 1 diabetes rat model

3.1.1 Confirmation of diabetes and development of neuropathic phenotype

In the STZ induced type 1 model studies conducted by Dr Lisa Lione and PhD candidate Michael Lanigan blood glucose levels (BGL) were measured to assess progression and maintenance of hyperglycaemia. One animal with a BGL <16mmol/dL was excluded from statistical analysis as it was deemed, they had not developed hyperglycaemia and become diabetic. The development of mechanical allodynia, phenotypical of neuropathic pain, was quantified through von Frey testing. 1 STZ animal with a <50% change from average baseline (day -7,-4) vs average neuropathic (day 9,11) and 1 control animal with a >50% change during von Frey testing were excluded from analysis. Figure 11 illustrates the reduction in von Frey paw withdrawal threshold in animals after STZ administration, thereby showing the development of mechanical allodynia in the STZ treated animals. In the 7-week study (figure 11A) STZ gradually caused a decrease in paw withdrawal threshold, the deficit was then maintained from day 7 onwards when comparing STZ and control animals. At 7 weeks and the completion of the study there was a statistically significant decrease in paw withdrawal threshold between control and STZ administered animals ($p < 0.001$). Similarly in the 4-week trial (figure 11B) at day 8 post STZ administration a deficit in withdrawal threshold developed which was maintained until the end of the study. Again at 4 weeks and the completion of the study there was a statistically significant decrease in paw withdrawal threshold between control and STZ administered animals ($p < 0.001$).

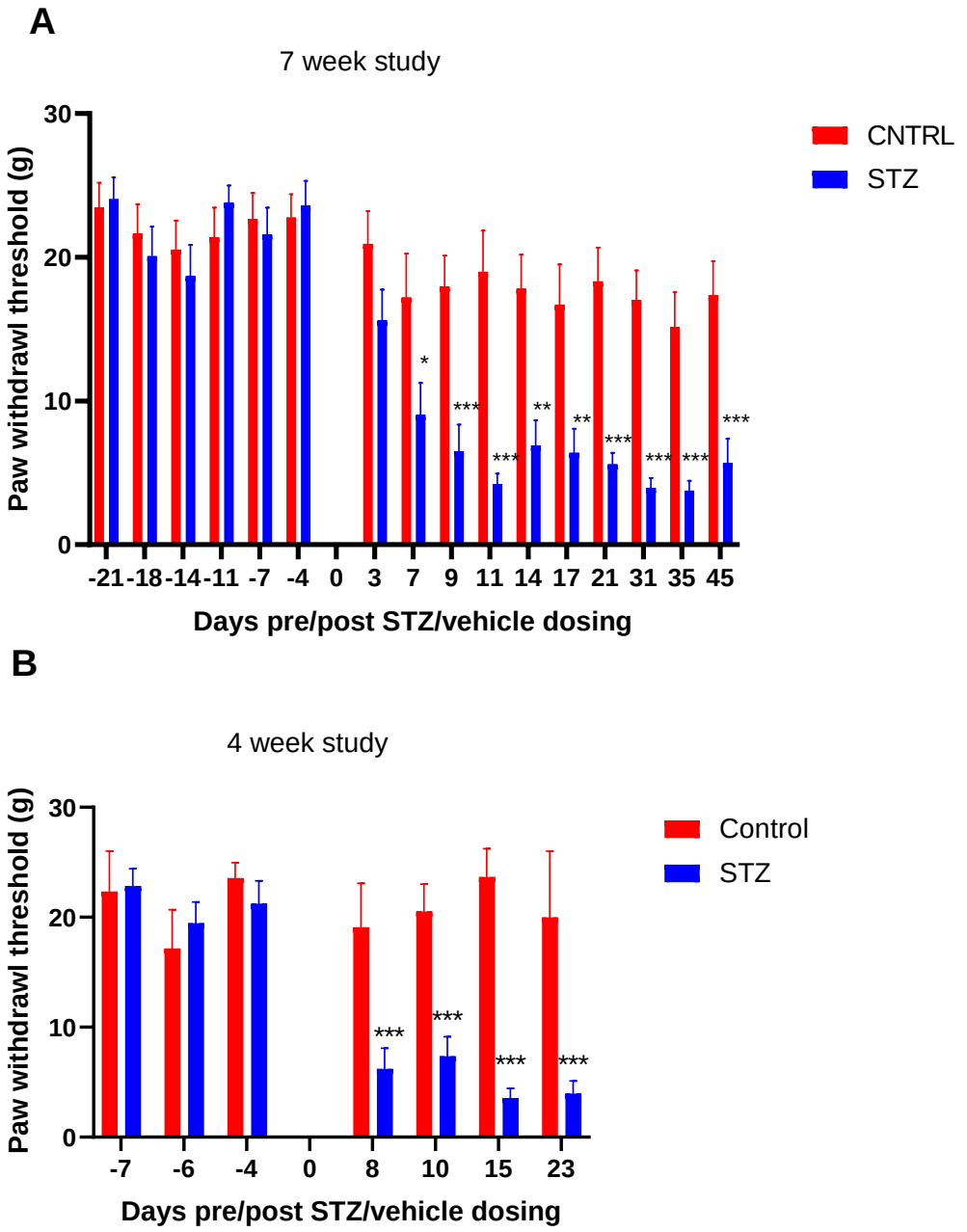

Figure 11. Development of mechanical allodynia assessed by von Frey paw withdrawal threshold using 0.4-26g hair range before and after STZ/vehicle dosing. (A) Development of allodynia in control (n=11) and STZ (n=14) in study running for 45 days after administration of STZ/vehicle. (B) Development of allodynia in control (n=4) and STZ (n=12) in study running for 23 days after administration of STZ/vehicle. Data presented as mean ± SEM; Asterisks indicate significant difference determined using multiple comparison two-way ANOVA: *p < 0.05, **p < 0.01, ***p < 0.001, significantly different from STZ (between group).

3.1.2 Alterations in intra epidermal nerve fibre density

In the rat plantar skin harvested from the STZ induced type 1 diabetes model studies IENFs were intensely immunostained by PGP 9.5. Figure 12 shows normal innervation and expression of Langerhans cells in plantar skin from a healthy control animal, whilst figure 13 depicts stating found in a diabetic rat 7 weeks after STZ administration. In the diabetic plantar skin, there is an increased number of LCs present and the IENFs become visibly smaller in size with less branching.

The linear density of IENFs was quantified at different time points in glabrous skin from the hind paw of healthy and STZ induced type 1 diabetic Wister Han ISG rats. In healthy control rats the average IENFD were 37.29 ±5.11, 33.76 ±2.71, and 36.56 ±4.36 (fibres/mm) at 2, 4, and 7 weeks respectively. In STZ treated animals the densities were 31.02 ±5.06, 31.45 ±3.66, and 28.96 ±3.69 (fibres/mm) at 2, 4, and 7 weeks respectively. A significant decrease in IENFD between control and STZ induced type-1 rats was found at 2- weeks($p<0.001$), and 7- weeks ($p<0.001$) fitting the expected hypothesis (Figure 14A and 14B). However no significant difference was seen at the 4-week timepoint ($p=0.0942$) (figure 14C). This is unexpected and is could be caused by anomalies arising from natural variation in the number of nerve fibres present in each animal and the small sample size.

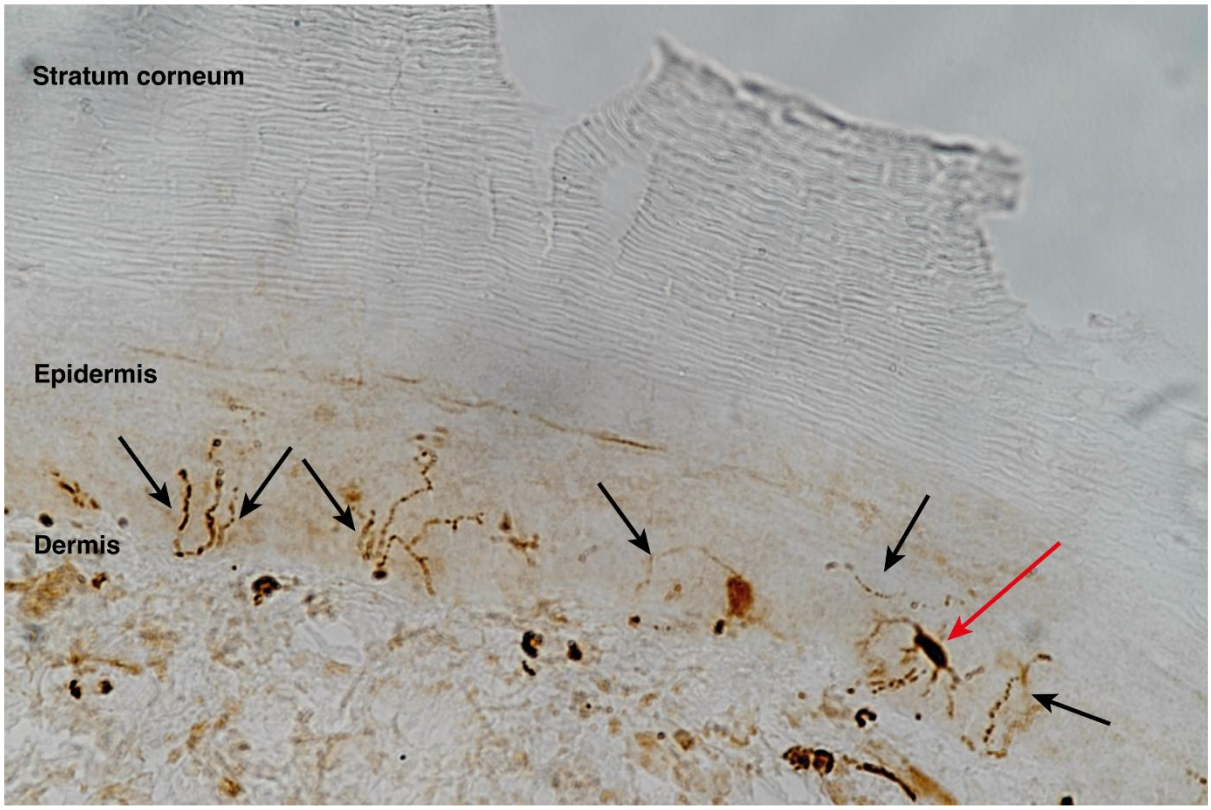

Figure 12. Normal innervation of hind paw footpad in healthy male Wister Han ISG rat stained with anti PGP 9.5 antibody at 40x magnification. Black arrows indicate intraepidermal nerve fibres, red arrow indicates PGP 9.5-positive Langerhans cells.

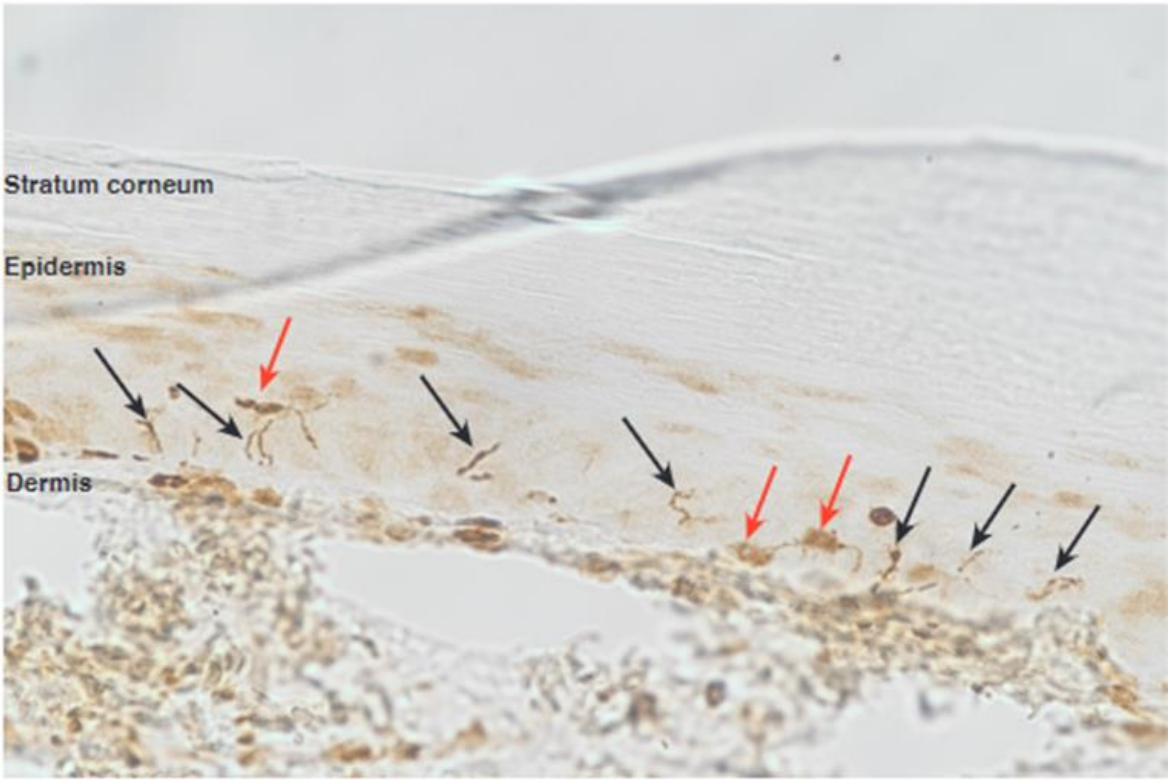

Figure 13. Innervation of hind paw footpad in diabetic male male Wister Han ISG rat 7 weeks after STZ administration stained with anti PGP 9.5 antibody at 40x magnification. Black arrows indicate intraepidermal nerve fibres, red arrow indicates PGP 9.5-positive Langerhans cells

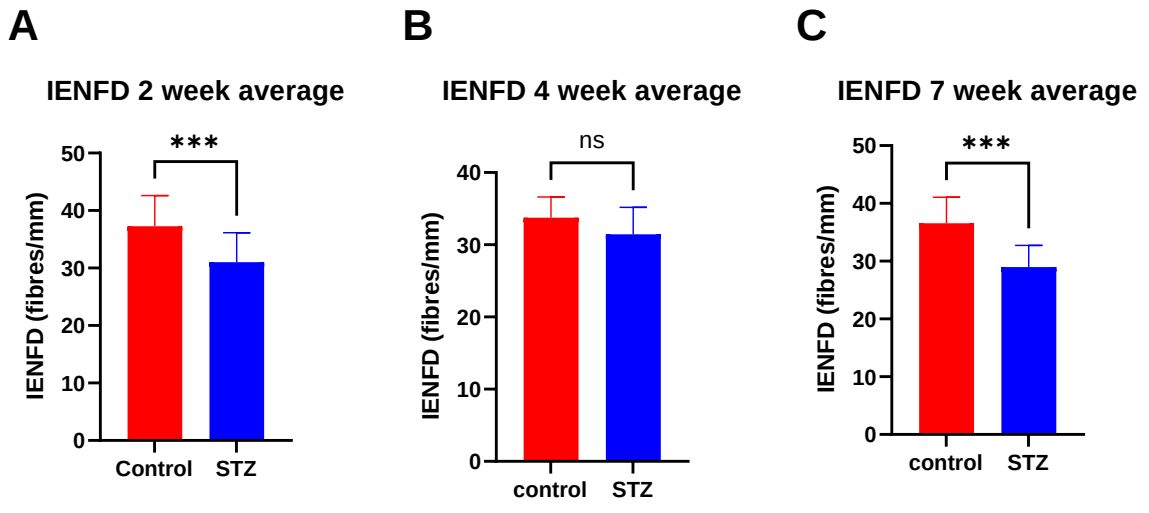

Figure 14. Intraepidermal nerve fibre density (IENFD) changes between control and STZ induced type-1 diabetic rats at 2-, 4- , and 7- weeks after STZ administration. (A) IENFD in control (n=2) and STZ (n=5) rats at 2 weeks, (B) IENFD in control (n=2), and STZ (n=4) at 4 weeks, (C) IENFD in control (n=3) and STZ (n=6) rats at 7 weeks. Data presented as mean ± SEM; Asterisks indicate significant difference determined using an unpaired t test, two tailed: ***p < 0.001, ns - not significant.

Natural ageing processes cause damage and cell loss, but as this was a relatively short study the IENFD was not expected to change due to the rats aging. As expected, the number of IENFs in control rats remained consistent across the different time points with no significant differences being found amongst them (figure 15A). Thus, providing a good benchmark to compare the IENFDs of neuropathic pain phenotype animals to. Although a deficit in IENFD in STZ animals compared to controls was observed, there was no significant difference found in IENFD of STZ animals at 2-,4- , or 7-weeks (figure 15B). This is in line with the mechanical allodynia observed from the von Frey paw withdrawal threshold. As a deficit in paw withdrawal was seen and maintained from 7 days onwards post STZ administration, which didn't progressively decline, mirroring the decrease in IENFD in STZ animals compared to controls. Whilst not significant at 4 weeks there is a trend to decrease in IENFD in the control which may account for loss of treatment significance at this time point.

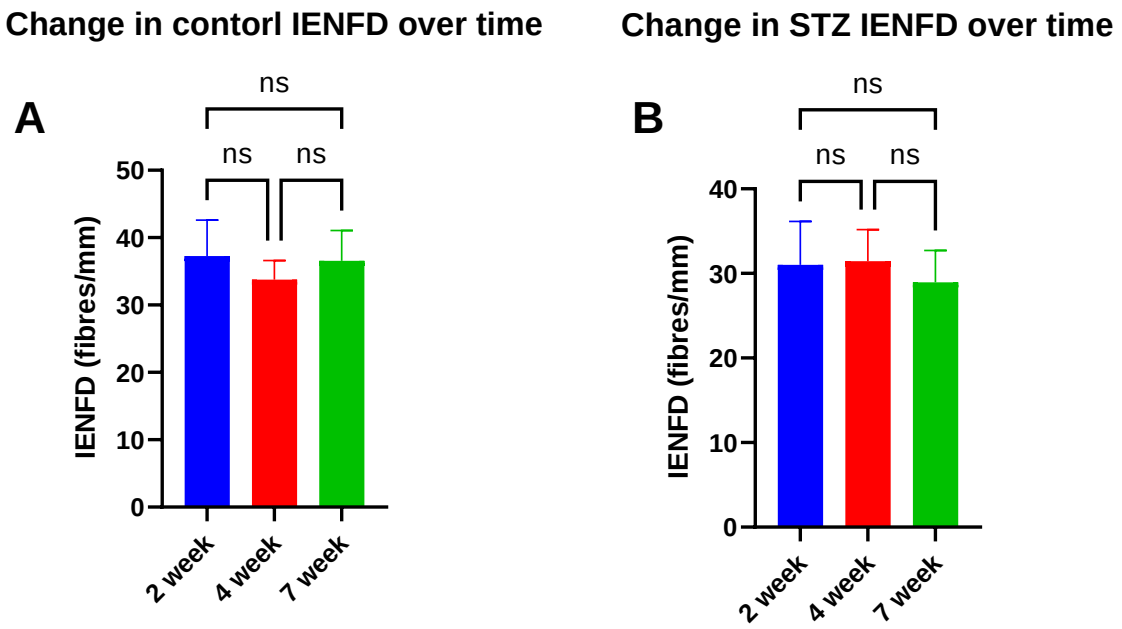

Figure 15. Changes in intraepidermal nerve fibre density (IENFD) over time. (A) Changes in IENFD in control rats at 2-, 4- and 7-week timepoints after vehicle dosing. (B) Changes in IENFD in control rats at 2-, 4- and 7-week timepoints after STZ dosing. Data presented as mean and ± SEM; Asterisks indicate significant difference determined using a one-way analysis of variance (ANOVA), two tailed: ns - not significant.

An ideal biomarker for neuropathic pain would not only indicate and confirm its presence but also be able to assess the progression of the disease. To evaluate this the IENFD of control and STZ animals was compared and correlated to their von Frey paw withdrawal threshold (figure 16). A significant positive corelation between the number of IENFs and paw withdrawal threshold was found ($r= 0.57$; $p<0.005$). Figure 16 again depicts how control animals have higher paw withdrawal thresholds and IENDS compared to those administered with STZ. Many points follow the trend and fall close to the linear regression line with the exception for one STZ animal which has a low IENFD but a high paw withdrawal threshold.

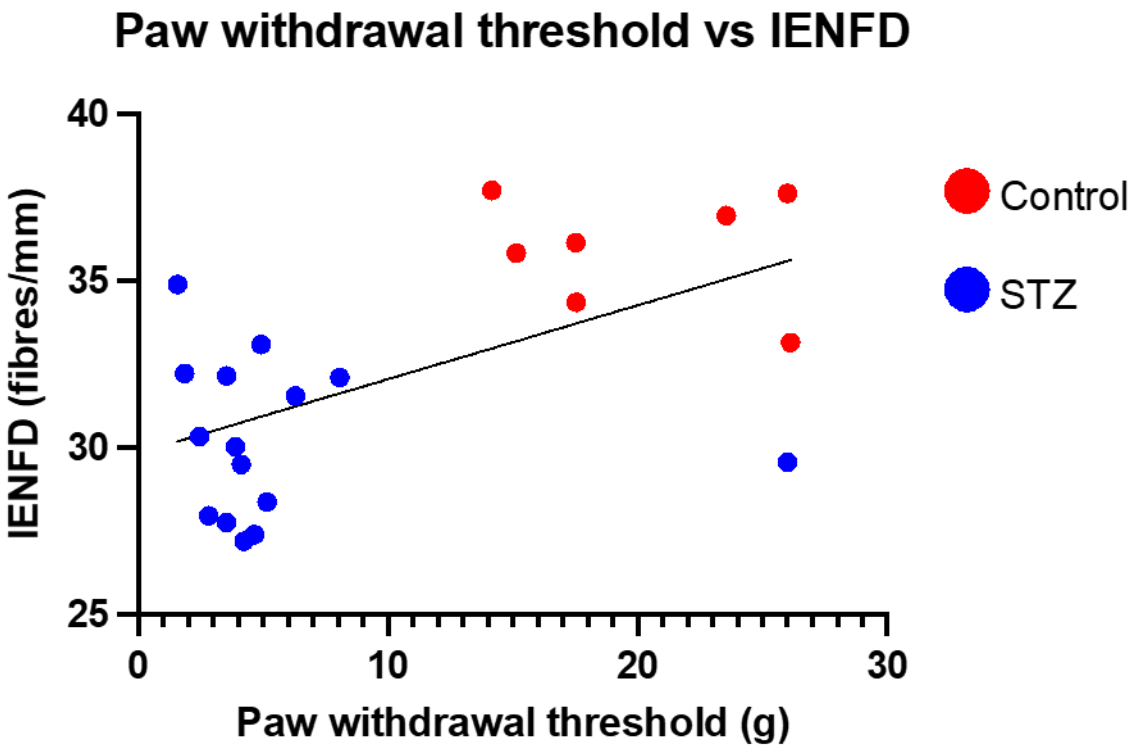

Figure 16. Correlation between intraepidermal nerve fibre density (IENFD) and paw withdrawal threshold in control and neuropathic rats ($r= 0.57$; $p<0.005$).

3.1.3 Increased Langerhans cells expression in diabetic rats

As it is speculated that LCs may play a role in the sensitisation of nociceptive terminals and in the generation and maintenance of neuropathic pain, LCs were intensely immunostained by PGP 9.5 and their linear density was quantified at different time points in glabrous skin from the hind paw of healthy and STZ induced type 1 diabetic Wister Han ISG rats (figure 17). In healthy control rats the average LC density were 3.77±0.72, 3.75±1.19, 4.37±0.48 (cells/mm) at 2, 4, and 7 weeks respectively. In STZ treated rats the average LC density were 8.31±0.50, 9.21±0.53, and 9.14± 0.74 (cells/mm) at 2, 4, and 7 weeks respectively. There was a statistically significant increase in the density of LCs between control and STZ treated rats at all timepoints ($p= <.001$). Between the 2-, 4-, and 7- week time points there was no significant change in LC expression in the control group and the STZ group ($p>0.05$) (Figure 18). There was an initial increase in LC density in the STZ group compared to the control group which remained consistent across the different time points.

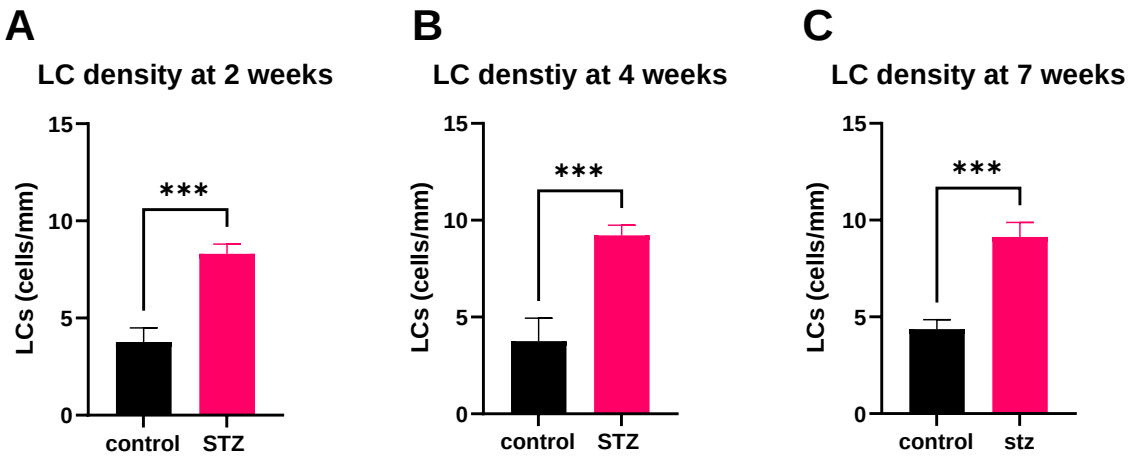

Figure 17. Langerhans cell density changes between control and STZ induced type-1 diabetic rats at 2-, 4- , and 7- weeks after STZ administration. (A) LC density in control (n=2) and STZ (n=5) rats at 2 weeks, (B) LCs in control (n=2), and STZ (n=4) at 4 weeks, (C) LCs in control (n=3) and STZ (n=6) rats at 7 weeks. Data presented as mean ± SEM; Asterisks indicate significant difference determined using an unpaired t test, two tailed: ***p < 0.001

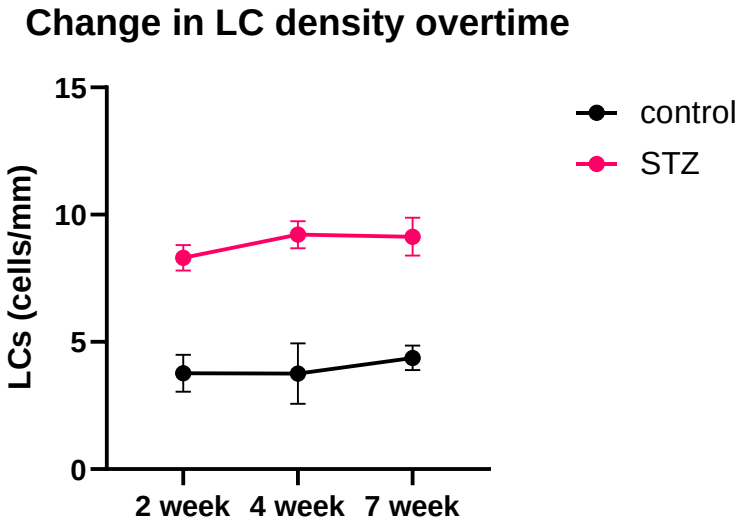

Figure 18. Change in LC cell density at 2-, 4-, and 7- week timepoints. No significant difference was determined in the control group across the time points or the STZ group across the timepoints. (p>0.05)

3.1.4 Negative correlation between IENFD and LCD

A negative correlation between the IENFD and LCD was found (r= -0.6214, p= <0.002) (Figure 19). As the number of IENFs increased the number of LCs decreased. Figure 7 further illustrates that control

rats were more likely to have a low number of LCs and a higher number of IENFs compared to STZ treated rats.

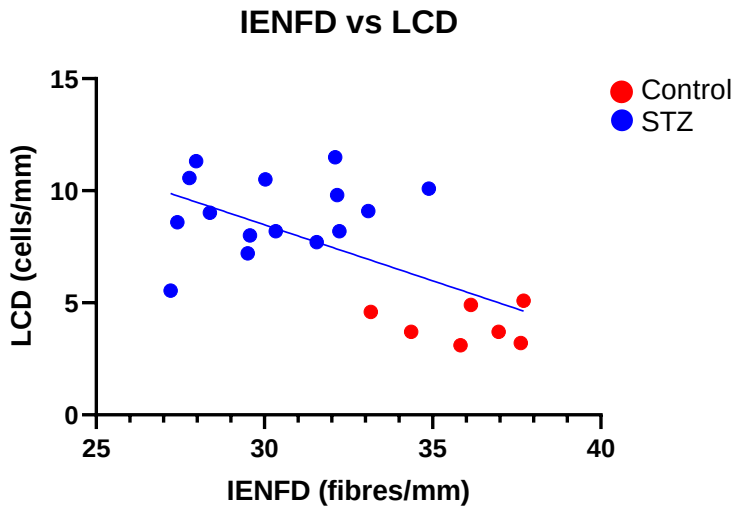

Figure 19. Correlation between intraepidermal nerve fibre density and Langerhans cell density in control and STZ treated rats (r= -0.6214, p= <0.002).

3.1.5 Proportional increase in cGRP immunoreactivity in diabetic rats

Skin innervation is a dynamic process and changes in overall nerve fibre density have been observed. Peptidergic nerve fibres also express TrkA, a receptor for nerve growth factor (NGF), which regulates neuropeptide expression. NGF-Trka signalling pathway has been implicated in pain generation and maintenance through changes in expression of peptides and receptors such as cGRP (Evans et al, 2012). These changes could potentially be used as an objective measure to identify and confirm the type and progression of pathological process such as neuropathic pain. For this reason, rat plantar skin harvested from the STZ induced type 1 diabetes model studies were intensely immunostained by cGRP (figure 20). The linear density of cGRP immunoreactive profiles was quantified at different time points in glabrous skin from the hind paw of healthy and STZ induced type 1 diabetic Wister Han ISG rats.

In healthy control rats the average cGRP reactive IENFDs were 1.95±0.25, 2.10±0.24, and 2.37±0.22 (fibres/mm) at 2, 4, and 7 weeks respectively. In STZ treated animals the average densities were 2.01±0.21, 2.57±0.24, and 2.45±0.27 (fibres/mm) at 2, 4, and 7 weeks respectively. No significant difference in the density of cGRP immunoreactive profiles was found between control and STZ type 1 induced diabetic animals at any time point (figure 21A, B, and C). There was also no significant difference found within the groups at the different time points (figure 21D).

Although there wasn't an observed increase in the actual number of cGRP reactive fibres between control and diabetic rat plantar skin there was an increase in the percentage of cGRP reactive fibres as a proportion of the total number of IENFs present in diabetic tissue compared to control (Figure 22). There was a significant increase in the percentage of IENFs immunoreactive to cGRP at 2 weeks from 5.69% in controls to 13.12% in diabetic rats (p=0.012). There was also an increase in CGRP percentage at 4 weeks, 5.56% in controls and 8.69% in diabetic rats, and at 7 weeks, 6.73% in controls and 9.12% in diabetic rats. However, the increase observed at 4 and 7 weeks wasn't found to be significant.

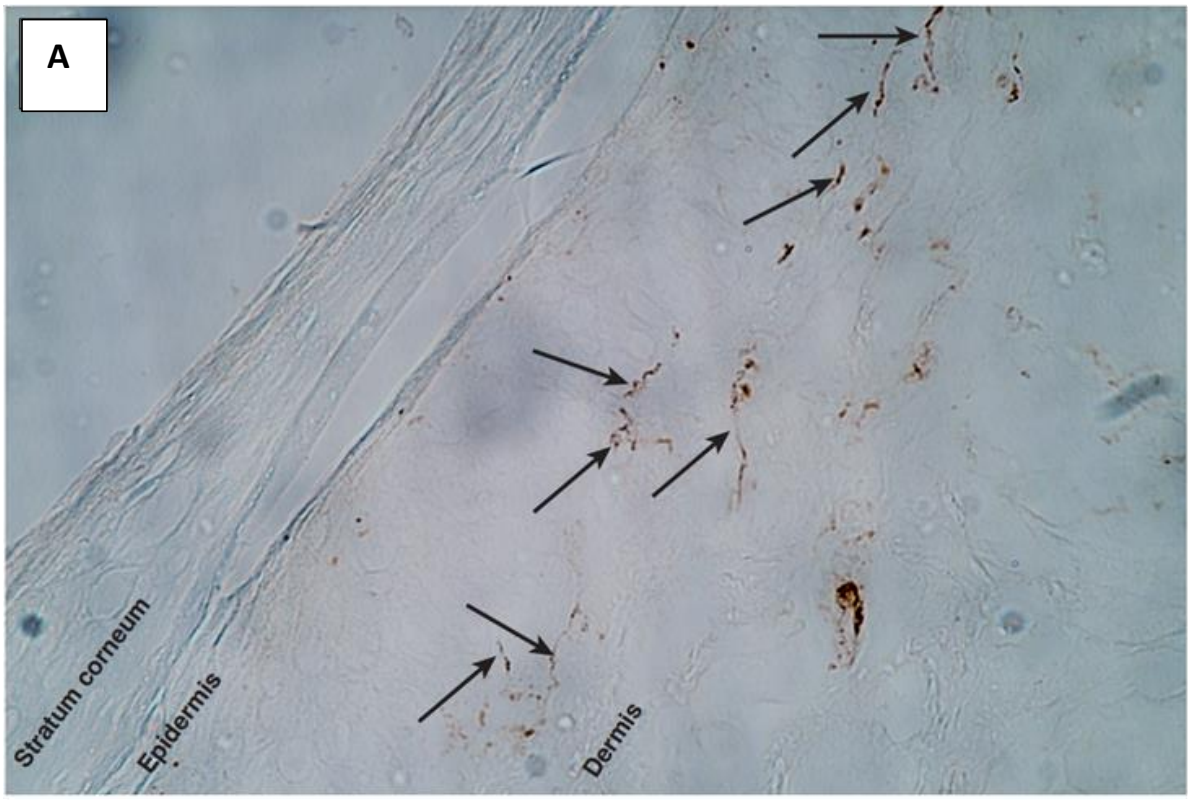

Figure 20. innervation of hind paw footpad in healthy male Wister Han ISG rat stained with anti cGRP antibody at 20x magnification. Black arrows indicate intraepidermal nerve fibres.

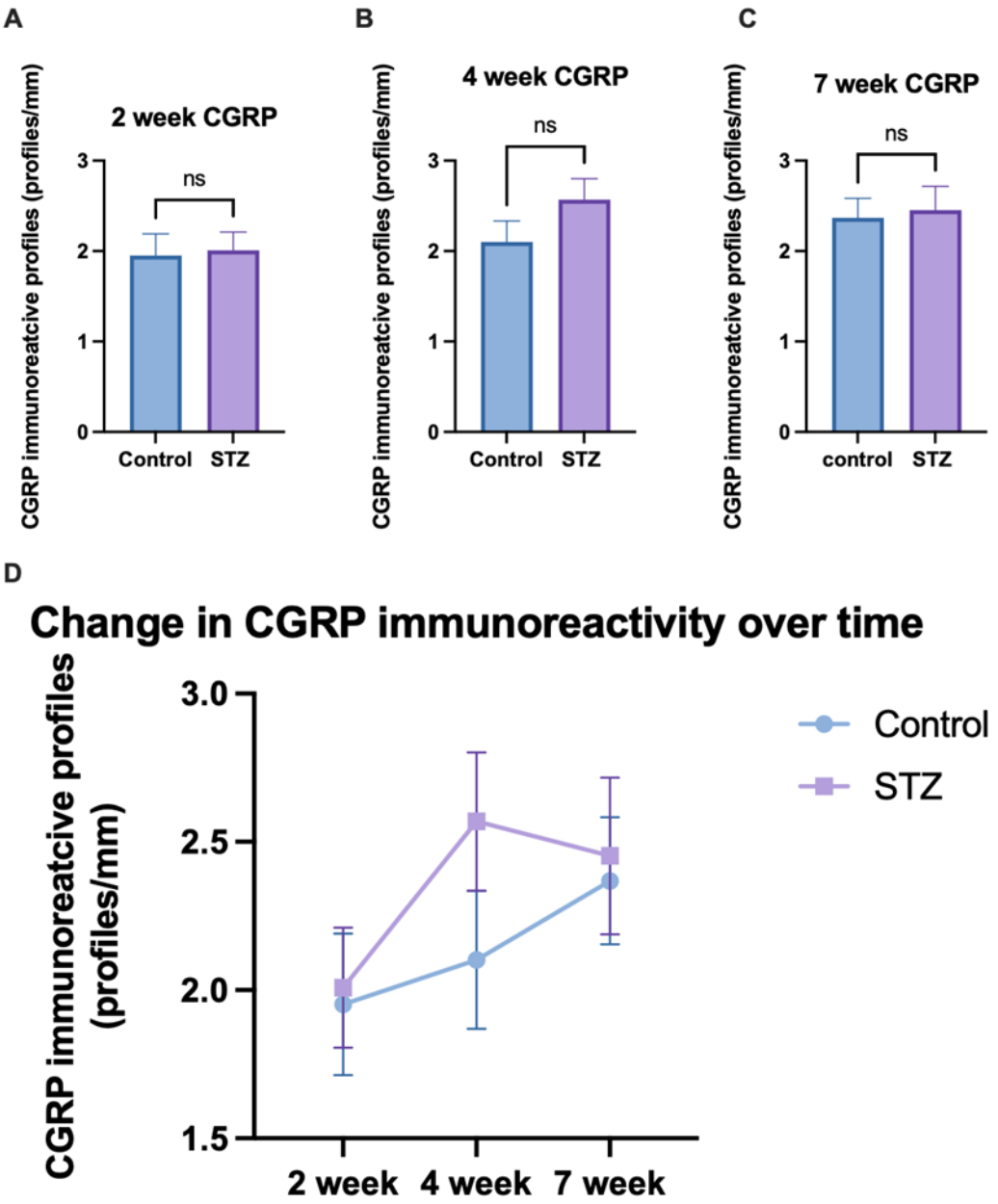

Figure 21. cGRP reactive IENFD changes between control and STZ induced type-1 diabetic rats at 2-, 4- , and 7- weeks after STZ administration. (A) cGRP density in control (n=2) and STZ (n=5) rats at 2 weeks, (B) cGRP density in control (n=2), and STZ (n=4) at 4 weeks, (C) cGRP density in control (n=3) and STZ (n=6) rats at 7 weeks. (D) Change in cGRP density at 2-, 4-, and 7- week timepoints. Data presented as mean ± SEM; Asterisks indicate significant difference determined using an unpaired t test, two tailed (A, B, C), two may multiple comparison ANOVA (D): *p < 0.05, **p < 0.01, ***p < 0.001, ns - not significant.

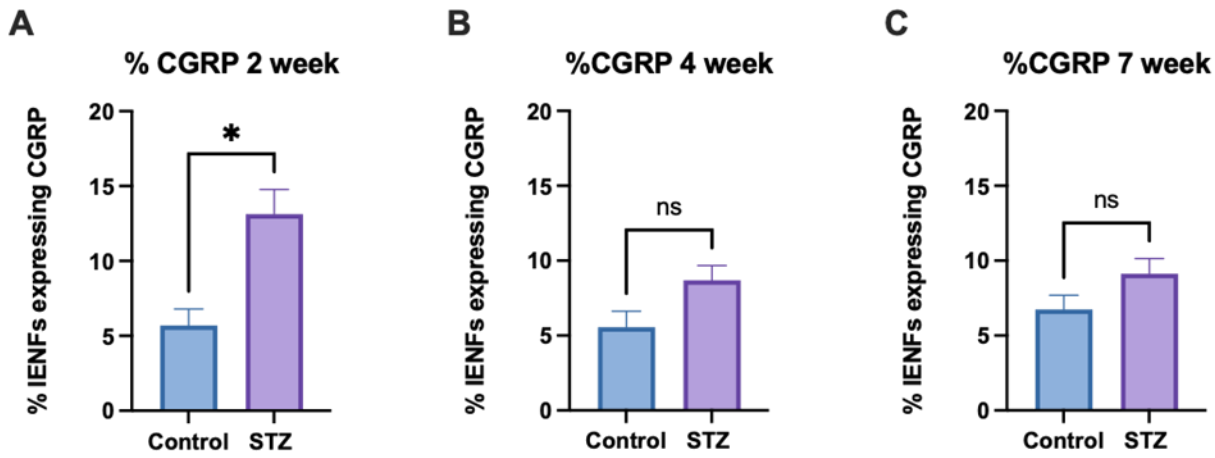

Figure 22. Percentage of IENFs being immunoreactive to cGRP in control and STZ induced type-1 diabetic rats at 2-, 4- , and 7- weeks after STZ administration. (A) % cGRP in control (n=2) and STZ (n=5) rats at 2 weeks, (B) % cGRP in control (n=2), and STZ (n=4) at 4 weeks, (C) % cGRP in control (n=3) and STZ (n=6) rats at 7 weeks. Data presented as mean ± SEM; Asterisks indicate significant difference determined using an unpaired t test, two tailed: *p < 0.05, **p < 0.01, ***p < 0.001, ns - not significant.

3.1.6 VEGF protein quantification in rat retina

There is an evident angiogenic paradox in diabetes, as there are a number of diabetic complications associated with impaired angiogenesis (neuropathy, wound healing) but also increased angiogenesis (retinopathy) (Costa & Soares, 2013). Whilst sensory neuronal expression of VEGF decreases in STZ diabetic rats, the total VEGF plasma levels are raised in symptomatic diabetic neuropathy (Pawson et al., 2010; Deguchi et al., 2009). In order to assess the potential change in VEGF expression in the retina of diabetic rats 4 weeks after STZ administration compared to healthy rat's western blot was used to quantify the protein concentrations. iBright™ Prestained Protein Ladder was used as a molecular weight marker which has chemiluminescent bands at 30kDa and 80kDa (Figure 23). Protein transfer was confirmed using the loading control GAPDH, this produced signals in all lanes at around 36kDa (Figure 23 B). Using the VEGF primary antibody, no signals were detected, other than the protein ladder (Figure 23 A).

Figure 23. western blot of cell lysate from control and STZ induced type 1 diabetes rat retina. (A) VEGF protein quantification using anti VEGF antibody. (B) protein quantification using GAPDH as a loading control which produced signals in all lanes

3.2 High fat diet induced type-2 diabetes mouse model

3.2.1 Confirmation of diabetes and neuropathic pain: Nottingham Trent University

In the high fat diet induced type 2 diabetes study run by Dr Richard Hulse and PhD candidate Lydia Hardowar at Nottingham Trent University the progression and maintenance of hyperglycaemia and the onset of diabetes in the mice blood glucose levels were monitored before and throughout the 12-week stud. Behavioural assessment of pain was evaluated using von Frey hairs (mechanical withdrawal) and Hargreaves test (thermal withdrawal) (figure 24). Both female and male mice fed the 42% and 60% fat diet had increased weight compared to the control chow group by the end of the study. There was increased blood glucose levels in the male 42% and 60% fat diet groups and 60% female group compared to the control chow group, suggesting these animals had become diabetic. In male and female mice on the 60% HFD diet they had significantly increased blood glucose levels ($p<0.05$). In male mice no difference in mechanical withdrawal threshold was found

using von Frey hairs between the different groups, with the thresholds remaining similar across the group's throughput the study. In contrast heat withdrawal threshold declined in the 42% fat diet and 60% fat diet in week 3 and remained lower for the majority of the study up until the termination of the study. In female mice mechanical withdrawal threshold remained steady in all groups up until week 6 were the control chow group increased and then cam back down and continued to fluctuate before returning to a similar level as was observed at the begging of the study. The 42% and 60% fat diet also remained steady and then fluctuated up at week 9 before declining each week until the end of the study. With both high fat diet groups having lower mechanical withdrawal threshold compared to the control at the end of the study. Heat withdrawal threshold in females across groups had similar values up until week 6 where the 60% fat diet groups latency began to decline up until the end of the study. The 42% fat diet groups latency began to decline around week 8 and at the end of the study both the 62% and 40% fat diet groups had lower heat withdrawal latency's then the control chow group. In male and female mice on the 60% HFD there was significantly lower heat withdrawal latency compared to control ($p<0.006$).

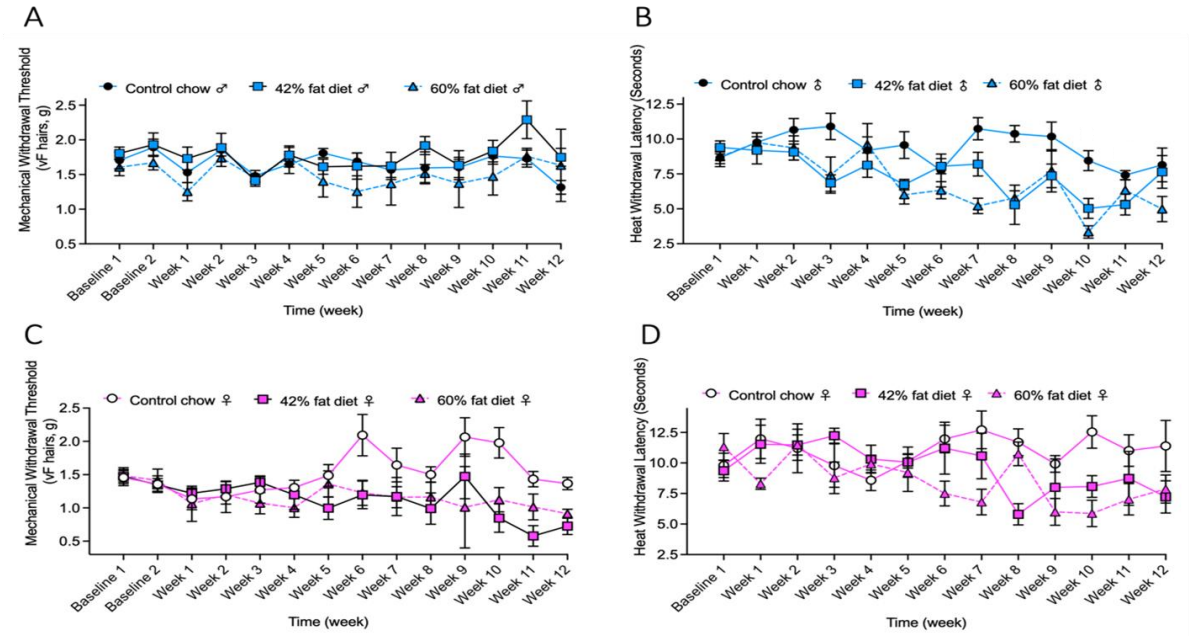

Figure 24. Behavioural assessment of mechanical and thermal allodynia using von Frey hairs and Hargreaves test in male and female C57 BI6 mice fed on either control chow male n=3, female n=3), 42% fat diet (male n=3, female n=3), or 60% fat diet (male n=3, female n=3). (A) Mechanical withdrawal threshold measured using von Frey hairs in male mice, (B) heat withdrawal latency measured using Hargreaves test in male mice. (C) Mechanical withdrawal threshold measured using von Frey hairs in female mice, (D) heat withdrawal latency measured using Hargreaves test in female mice.

3.2.2 Changes in intra epidermal nerve fibre density

In mouse plantar skin, harvested from the high fat diet induced type 2 diabetes model study, IENFs were intensely immunostained by PGP 9.5 (figure 25 and 26). The linear density of IENFs was quantified in male and female mice fed for 12 weeks on either control chow, 42% fat diet, or 60% fat diet (figure 27). In healthy control chow fed mice the average IENF density was 33.56±4.60 fibres/mm in male mice and 32.90±3.92 fibres/mm in female mice. Male mice fed the 42% fat diet had an average IENF density of 32.07±2.58 and in females it was 28.31±3.29 fibres/mm. Male mice

fed on the 60% chow diet had an average IENF density of 27.92±4.55 fibres/mm in male mice and 26.06±3.32 fibres/mm in female mice.

No significant difference was found in male mice fed on control chow or 42% fat diet. There was however a significant decrease in IENFD between male mice fed control chow and those fed 60% fat diet ($p < 0.001$) as well as between male mice fed 42% and 60% fat diet ($p=0.010$). In female mice there was a significant decrease in IENFD from the control chow group in both the 42% fat diet group ($p=0.002$) and the 60% fat diet group ($p < 0.001$). This is in line with male and female mice on the higher percentage fat diets developing hyperglycaemia and diabetes, as determined my blood glucose levels. Which also correlates to the neuropathic pain phenotype behaviour displayed by male mice on the 60% fat diet displaying lower heat withdrawal latency.

Male mice and female mice fed the control chow had similar IENFDs, this was also true for the 60% fat diet. However, on the 42% fat diet female mice IENFD was significantly lower than that of the males. Although this is likely due to the small n number and natural variance in nerve fibre density it is possibly a sign that females are more susceptible to the development of neuropathy and neuropathic pain. This is something which is observed in the general population with chronic neuropathic pain having a frequency of 8% in women versus 5.7% in males (Bouhassira et al., 2008).

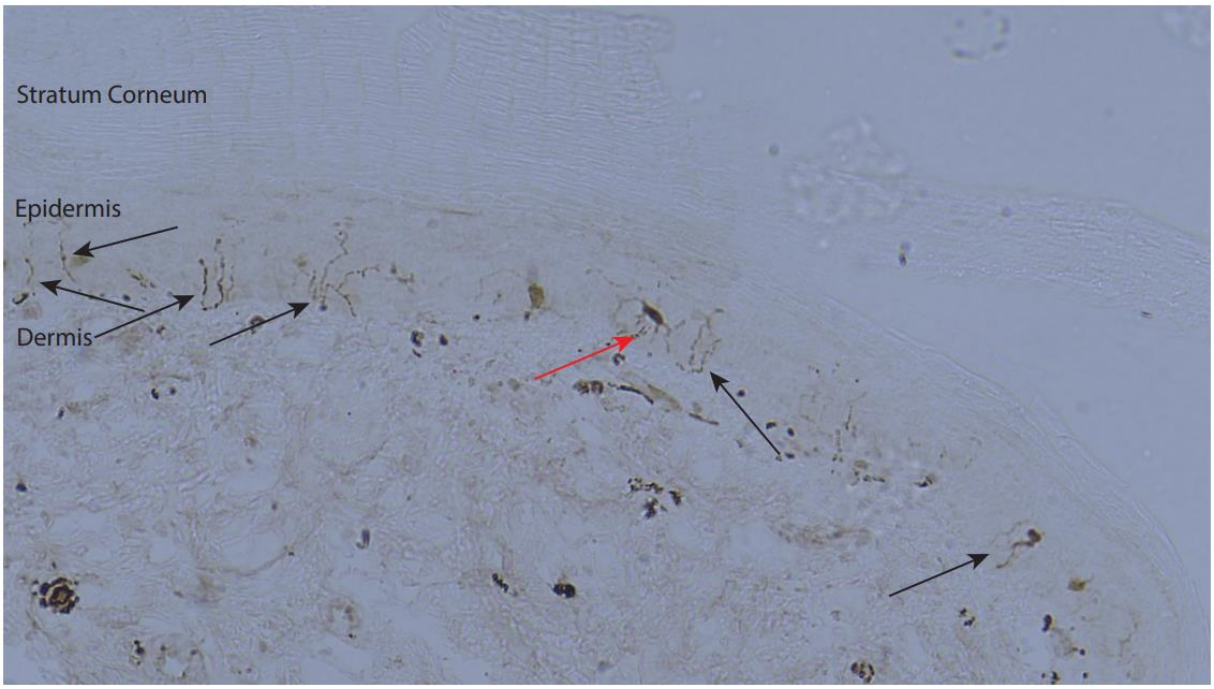

Figure 25. Normal innervation of hind paw footpad in healthy male C57 BI6 mouse stained with anti PGP 9.5 antibody at 20x magnification. Black arrows indicate intraepidermal nerve fibres, red arrow indicates PGP 9.5-positive Langerhans cells.

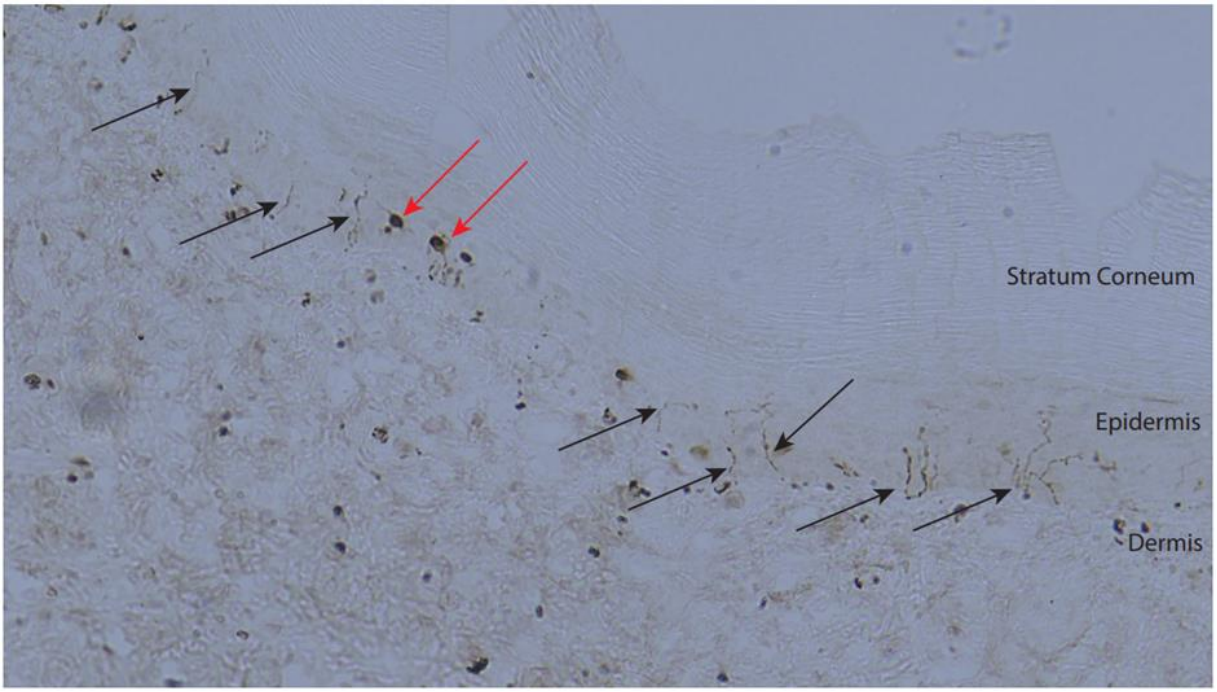

Figure 26. Innervation of hind paw footpad in male C57 BI6 mouse fed 60% fat diet stained with anti PGP 9.5 antibody at 20x magnification. Black arrows indicate intraepidermal nerve fibres, red arrows indicate PGP 9.5-positive Langerhans cells.

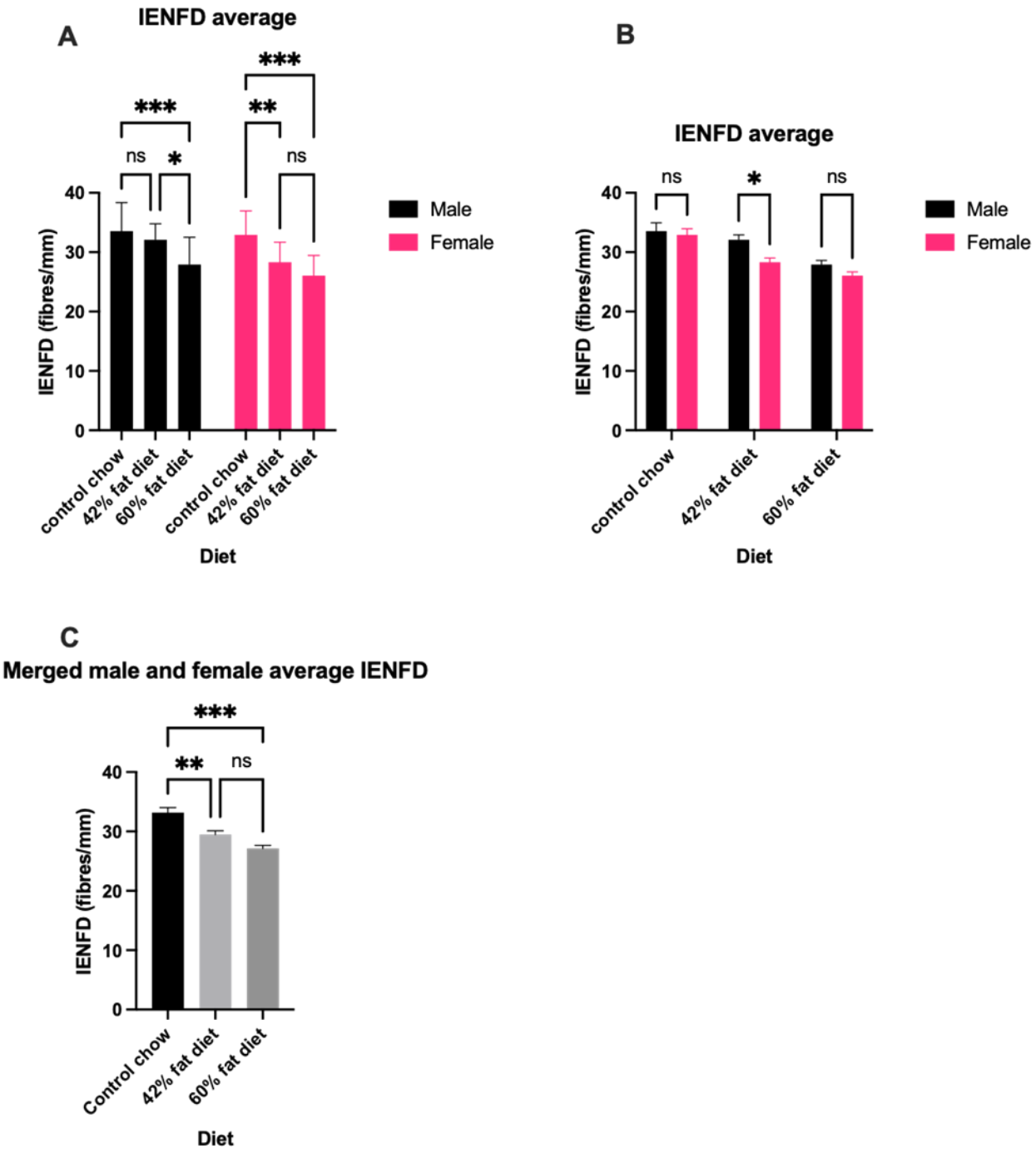

Figure 27. Intra epidermal nerve fibre density changes in male and female mice fed for 12 weeks on control chow (male n=3, female n=3), 42% fat diet (male n=3, female n=3), and 60% fat diet (male n=3, female n=3). A) The change in IENFD between animals of the same sex fed difference fat percentage diets. B) The change in IENFD between male and female mice fed on the same fat percentage diets. C) IENFD change dependent on diet when male and female mice data is grouped together. Data presented as mean ± SEM; Asterisks indicate significant difference determined using two may ANOVA: *p < 0.05, **p < 0.01, ***p < 0.001, ns - not significant.

3.2.3 Langerhans cell expression in control vs diet induced type 2 diabetic mice

LCs were intensely immunostained by PGP 9.5 and their linear density was quantified in glabrous skin from the hind paw of mice fed control chow, 42% fat diet, and 60% fat diet (figure 28). In healthy control chow fed mice the average LC density was 3.39 cells/mm in male mice and 3.38 cells/mm in female mice. Male mice fed the 42% fat diet the average LC density was 3.57 and in females it was 4.11 cells/mm. Male mice fed on the 60% chow diet had an average LC density of 3.97 cells/mm in male mice and 4.50 cells/mm in female mice. No significant difference was found between the male and female mice fed the same diet. Although there was a small increase in LC density as the fat percentage of the diets increased from control chow to 42% to 60% fat, no significant increase was found. There was also no significant correlation found between IENFD and LC density in density in male and female control, 42% HFD, and 60% HFD mice ($p=0.255$, $R^2=0.079$) (Figure 29).

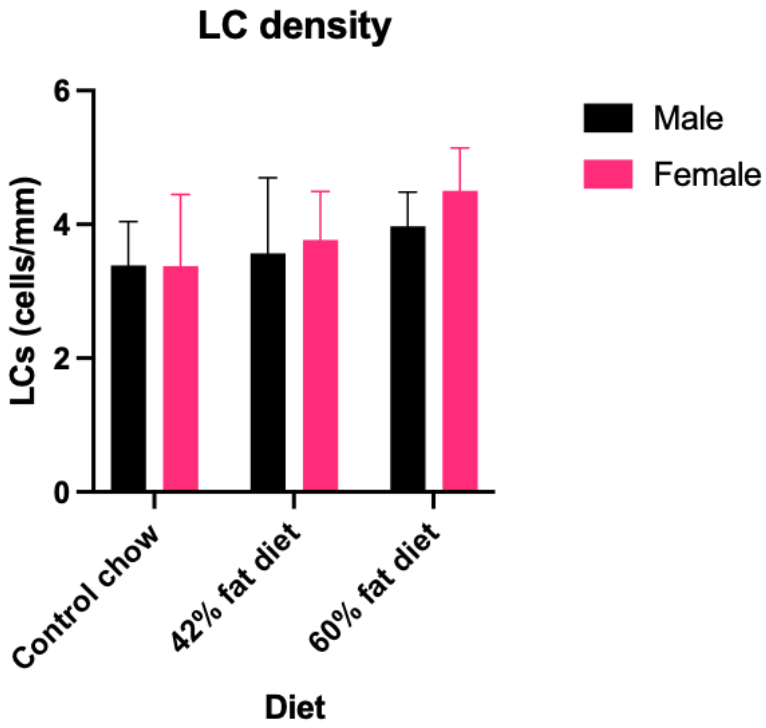

Figure 28. Langerhans cell density changes in male and female mice fed for 12 weeks on control chow, 42% fat diet, and 60% fat diet. Data presented as mean ± SEM; no significant difference was determined using two-way ANOVA.

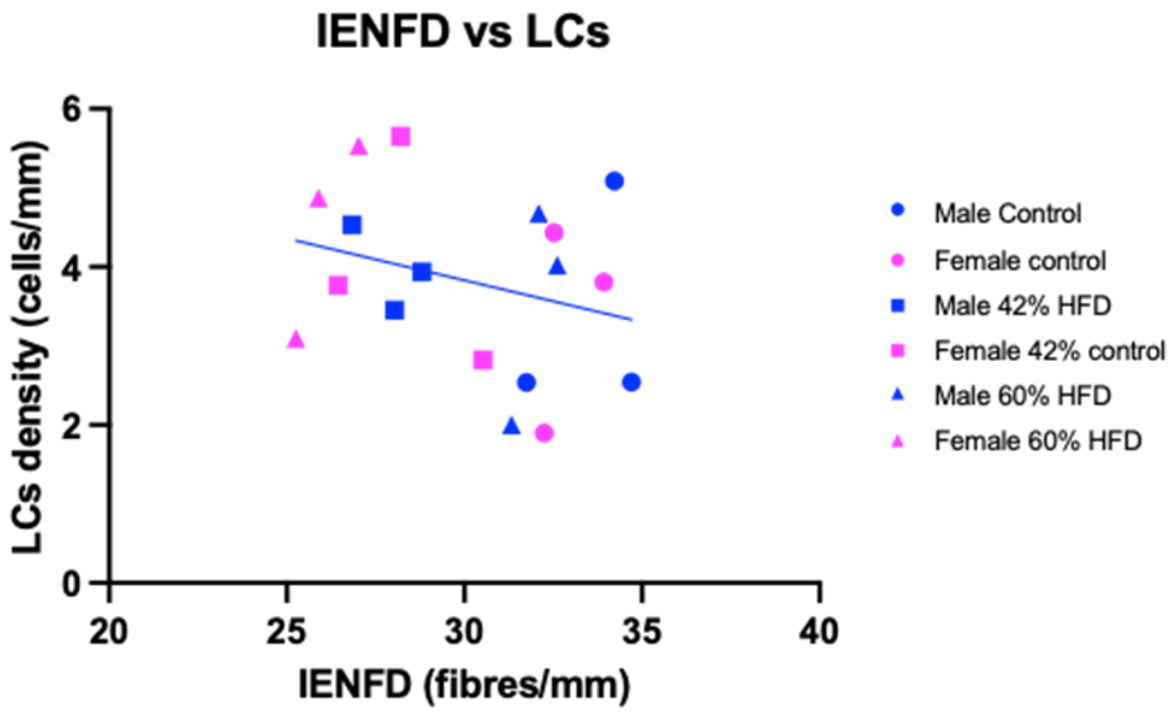

Figure 29. Correlation between intraepidermal nerve fibre density and Langerhans cell density in male and female control, 42% HFD, and 60% HFD mice. No significant correlation was found ($p=0.255$, $R^2=0.079$)

3.3.3 No change in proportion of cGRP immunoreactive fibers in type 2 model

In mouse plantar skin, harvested from the high fat diet induced type 2 diabetes model study, cGRP immunoreactive IENFs were intensely immunostained by an anti cGRP antibody (figure 30 A). The linear density of cGRP reactive IENFs was quantified in male and female mice fed for 12 weeks on either control chow, 42% fat diet, or 60% fat diet. In healthy control chow fed mice the average cGRP reactive fibre density was 2.25 fibres/mm in male mice and 2.54 fibres/mm in female mice. Male mice fed the 42% fat diet had an average cGRP density of 2.23 and in females it was 2.20 fibres/mm. Male mice fed on the 60% chow diet had an average cGRP density of 1.99 fibres/mm in male mice and 2.09fibres/mm in female mice. In both male and female mice there was a slight decrease in cGRP fibre density as the fat percentage of the diet increased however no significance was found. Female mice had slightly higher average fibre densities compared to male mice in the control and 60% fat diet group, again this small difference was not significant.

There were no significant differences found when looking at the percentage of cGRP reactive fibres as a proportion of the total number of IENFs present in diabetic tissue between male and female mice and the different diet groups (figure 30 B). The percentage of IENFs immunoreactive to cGRP in mice fed control chow was 6.84% in males and 6.61% in females. There was a small negligible increase in mice fed on the 42% fat diet to 7.03% in males and 7.81% in females. Mice fed for 12 weeks on the 60% fat diet again had slightly higher averages then the control chow, 7.22% in male mice and 8.18% in females.

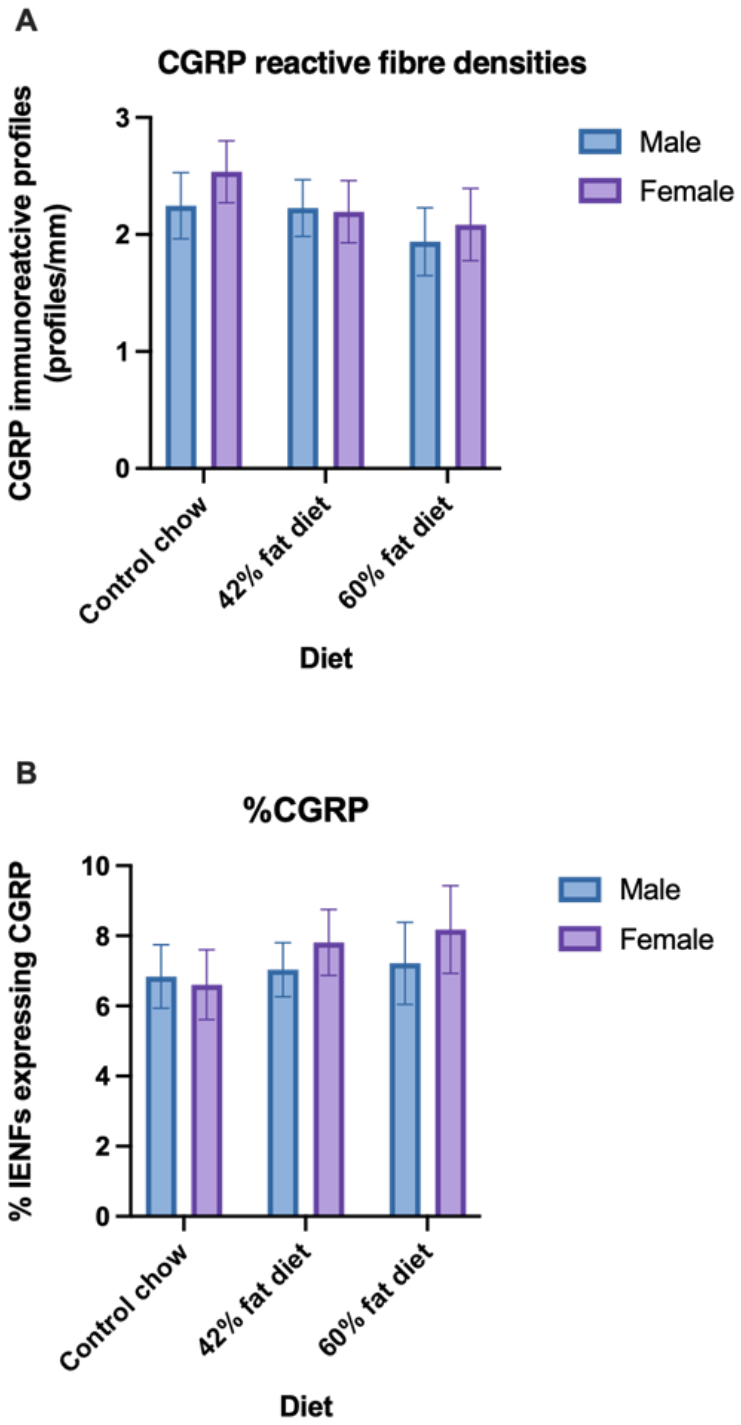

Figure 30. Changes in levels of CGPR immunoreactive IENFs in male and female mice fed for 12 weeks on either control chow (male n=3, female n=3), 42% fat diet (male n=3, female n=3), or 60% fat diet (male n=3, female n=3. (A) Density of cGRP reactive fibres. (B) Percentage of total IENFs being immunoreactive to cGRP. Data presented as mean ± SEM; no significant difference was determined using a two-way ANOVA

4. Discussion

4.1 Main findings

Diabetic peripheral neuropathy affects more than half of all diabetic patients, with neuropathic pain being the most common symptom (Obrosova, 2009). However, the underlying pathology is poorly understood resulting in only a small percentage of patients benefiting from current treatments options. This is compounded by poor translatability of drugs from positive preclinical results into successful human trials. Without biomarkers which effectively predict neuropathic pain, it is challenging to identify treatments preclinically for successful translation in humans. In this study immunohistochemistry was utilised to characterise peripheral neuropathy and biomarkers as predictors of neuropathic pain in preclinical models of type 1 and 2 diabetes. There was found to be a decrease in IENFD in diabetic animals across both models, and the IENFD correlated with mechanical allodynia observed in the STZ induced type 1 diabetes rat model but not HFD type 2 diabetes mouse model. An increase in LCs was present in diabetic animals in the STZ induced type 1 diabetes model, this increase strongly correlated to the decrease in IENFD, providing evidence that used in conjunction IENFD and LC density are reliable biomarkers of diabetic neuropathy in this model. cGRP reactivity also proportionally increased in STZ induced type 1 diabetic rats however no change was observed in the HFD induced type 2 diabetic mice, therefore was inconclusive as to the effectiveness of cGRP as a biomarker of neuropathy. No time course effects in IENFD decrease, LCs increase, or cGRP increase were found in 2-, 4-, and 7-week STZ induced type 1 diabetic rats.

4.2 Protocol development: Different processing methods and protocol limitations

Although IHC is a well-established technique it isn't without its disadvantages and limitations. The procedures and stains used aren't standardised and it can be hard to decipher what the best stains to use are. In addition, well-trained personnel with a high skill base are needed to eliminate human error. Due to the subjective nature of interpreting visual images, it can also be challenging to quantify results. To overcome these problems protocol optimisation steps were taken to develop high quality staining and robust quantification methods. Over several months of testing different variables such as: section thickness, microscope slide type, wash buffers, primary antibody concentrations, and antigen retrieval methods, a successful protocol was developed to stain rodent plantar skin with PGP 9.5 and cGRP. Whilst most problems were solved a few issues persisted. Tissue sections not fully adhering to the slide and falling off or becoming folded during washing steps was a common problem. This was especially apparent in FFPE tissue sections but occurred less in the cryoprotected tissue. Cryoprotected tissue were also faster to process, as paraffin embedding, and then subsequent deparaffinising steps could be emitted. Although FFPE tissue sections seemed to stain more intensely then cryoprotected tissue, the difference was minimal and very subjective, making both methods of processing equally adequate. In the protocol developed chromogenic stains were used which were visualised with a brightfield microscope. Chromogenic detection was preferred due to stained sections being more resilient to photobleaching compared to fluorescent staining, so slides could be re analysed in the future. It also meant morphological characteristics of the tissue were easier to observe. This was a consideration as the length, axonal width and appearance of the IENFs could have been analysed if time had permitted. However chromogenic detection meant that image analysis had to be done manually as the intensities of the

immunoreactive profiles couldn't be differentiated automatically. If immunofluorescence had instead been utilised it is possible that the analysis could have been done automatically in a software package such as ImageJ. This could have cut down on human error and made analysing the results much quicker and efficient.

Another issue which occurred during protocol optimisation was the wastage of tissue samples. To begin with plantar skin tissues were being embedded in paraffin and cut horizontal to the sagittal plane of the paw pad. Unfortunately, these slices had little value in quantifying nerve fibre density. Meaning these tissue samples were wasted. This included tissue from a STZ induced type 1 rat which had developed diabetes but no neuropathic pain phenotypical behaviour. Allowing for the potential to compare IENFD in a painful and painless neuropathy.

4.3 Decrease in intra-epidermal nerve fibre density in diabetic rodents

Skin biopsies are routinely used in human patients with neuropathies and neuropathic pain to assess the impaired function of small diameter IENFs (Griffin, McArthur, & Polydefkis, 2001). A technique which has proven to be diagnostically reliable and has shown correlation to the sensory symptoms of neuropathic pain resulting from the nerve fibre degeneration (Periquet et al., 1999). In rodent models of peripheral neuropathy and neuropathic pain, the quantification of IENFs has the potential to assess the development and potential severity of the neuropathy, as well as predict the extent of neuropathic pain. Although IENFs have been extensively studied in rodent plantar skin, quantitative data on IENFD in healthy control animals and data is especially limited in studies using an STZ indued type 1 diabetic model or HFD diet induced type 2 model, hence this research is novel (Stankovic, Johansson, & Hildebrand, 1996; Lin, Tseng, Lin, & Hsieh, 2001; Lauria et al., 2005; Andreasen et al., 2020). In this study the IENFD was quantified in healthy control male Wister Han ISG rats and in STZ induced type 1 diabetic rats after 2, 4 and 7 weeks, as well as in healthy control male and female C57 BI6 mice and HFD (42% aand 60%) induced type 2 diabetic mice after 12 weeks.

In this study it was observed that compared to the control group there was a significant reduction in IENFD in STZ induced type 1 diabetic rats at 2-, and 7- week time points ($p<0.001$) (figure 14). With the healthy vs STZ induced diabetic IENFDs values being 37.3±5.1 vs 31.0±5.1, 33.8±2.7 vs 31.5±3.7, and 36.7±4.4 vs 29.0 ±3.7 (fibres/mm) at 2, 4, and 7 weeks respectively (figure 14). This decrease in IENFD in STZ induced type 1 diabetic rats is in line with previous studies, and although due to the limited quantitative data available there is no exact reference figure for the IENFD in rat plantar skin and a large range of values have been published for PGP 9.5 IENFD, the observations in this study fall towards the top of previously reported data (Lauira et al., 2005; Hossain et a., 2020; Andreasen et al., 2020; Wang et al., 2019). Previous studies in rats have reported healthy control vs diabetic IENFDs of 21.6±4.8 vs 12.3±3.6 (Lauira et al., 2005), 9.0±2.5 vs 3.4±1.4 (Andreasen et al., 2020), and 35.2±2.8 vs 30.2±2.4 (Wang et al., 2019). Whilst most of the available literature agrees that there is a decrease in IENFD with the incidence of diabetes a 2013 study reported a 21% increase in IENFD in STZ induced diabetic rats (Sugimoto, Baba, Suzuki, & Yagihashi, 2013). In this study a similar dose of STZ (45mg/kg) was used compared to our model (55mg/kg), with the biggest difference being that the study carried on for 12-weeks after STZ administration compared to 2-, 4-, and 7-weeks. In STZ induced type 1 diabetic rats in the Sugimoto study the von Frey mechanical withdrawal threshold decreased significantly from 6 to 12 weeks compared to control rats ($p<0.05$), whilst the STZ induced type 1 diabetic rats, in the study conducted by Dr Lisa Lione and Micheal Lanigan, had stable withdrawal thresholds (mechanical allodynia) 1 week after STZ administration. Suggesting that although there was development of nociceptive dysfunction and functional abnormalities in these

STZ induced type 1 diabetic rats, there was no structural abnormalities to small sensory IENFs in this model.

The large range of reported IENFD values across rat models is most likely caused by differences in the counting method and the type of microscopy utilised. All the published studies counted the fibres as they crossed the dermal-epidermal junction, with secondary branching in the epidermis being excluded. However exact counting methods were not reported. Such as whether nerve profiles/fragments present only in the epidermis, and not seen crossing the dermal-epidermal boundary, were counted. If these are included this would lead to a higher reported value. In this study these were included to give a better representation of the overall number of nerve fibre profiles present (figure 7), however this could have potentially led to over counting, explaining why the IENFD in this study was higher compared to published reports. This quandary could have been remedied if confocal microscopy was implemented instead of traditional brightfield microscopy. Confocal microscopy would have allowed the staking of 2D images to produce a 3D image which would more clearly illustrate where nerve fibres originated, branched, and terminated, however traditional microscopy has been found to be just as reliable as confocal digital images for determining IENF density (Provitera et l., 2015). Whilst accurately reporting the number of nerve fibres is important the potential overcounting does not affect the validity of the data and subsequent conclusion made. Change in density and counting and reporting of IENFD is consistent enabling accurate comparisons across treatment groups.

A significant positive correlation between the number of IENFs and paw withdrawal threshold was noted ($r= 0.57$; $p<0.005$) (figure 19). Figure 19 clearly depicts how control animals (red dots) have higher paw withdrawal thresholds and IENFs compared to those with STZ induced type 1 diabetes (blue dots) and had phenotypical neuropathic pain behaviour. This is in line with observations in humans where IENFD correlates with thermal-thresholds, pressure sense and total neurological disability score (Pittenger et al., 2004; Shun et al., 2004). Collectively this suggests the STZ induced type 1 diabetes model used in this study is a suitable preclinical model, strengthening the argument that IENFD quantification is useful in assessing the development and potential severity of the neuropathy, as well as predict the extent of neuropathic pain.

There was also a significant decrease in IENFD observed in HFD induced type 2 diabetic mouse model at both 42% an 60% fat diet, yet the IENFD reduction was to a lesser extent than observed in the STZ induced type 1 diabetic rat model (figure 27). No significant IENFD difference ($p>0.05$) was noted in male mice fed on control chow, 33.6±4.6 fibres/mm, versus 42% fat diet, 32.1±2.6 fibres/mm. However, a significant decrease in IENFD between male mice fed control chow and those fed 60% fat diet, 27.9±4.6 fibres/mm, ($p < 0.001$) as well as between male mice fed 42% (32.1±2.6 fibres/mm) and 60% fat diet (27.9±4.6 fibres/mm) ($p=0.010$). In female mice there was a significant decrease in IENFD from the control chow group, 32.9±3.9 fibres/mm, in both the 42% fat diet group, 28.3±3.3 fibres/mm, ($p=0.002$) and the 60% fat diet group, 26.1±3.3 fibres/mm, ($p < 0.001$). This is in line with male and female mice on the 60% HFD diet having significantly increased blood glucose levels ($p<0.05$), along with male and female mice on the 60% HFD having significantly lower heat withdrawal latency compared to control ($p<0.006$).

Male and female mice fed the control chow had similar IENFDs ($p>0.05$), also true for male and female mice 60% fat diet ($p>0.05$). However, IENFD was significantly lower ($p<0.05$) in female mice 42% fat diet (28.31±3.29 fibres/mm) compared to that to the respective males (32.07±2.58 fibres/mm). Though this is likely due to the small sample size and natural variance in nerve fibre density, it is possibly a sign that females are more susceptible to the development of neuropathy and neuropathic pain. This is observed in the general population where chronic neuropathic pain

prevalence is 8% in women versus 5.7% in males (Bouhassira et al., 2008). Male mice fed 42% and 60% HFD did not show signs of mechanical allodynia in von Frey testing, there was in fact a slight increase in paw withdrawal compared to control (figure 19). Conversely in the STZ induced type 1 diabetes models STZ administered rats had a significant decrease in mechanical paw withdrawal threshold ($p < 0.001$) This may be due to the fact that STZ (50mg/kg ip) caused the onset of hyoerglycemia and subsequent mechanical allodynia (within 7 days, figure 11) and peripheral nerve fibre damage (within 2 weeks, figure 14), more rapidly than a HFD induced type 2 diabetes phenotype. Whilst speculative, it is also possibly due to mechanistic differences between how STZ induced type 1 and HFD induced type 2 diabetes peripheral neuropathy phenotype is generated.

4.4 Increase in Langerhans cell density in STZ induced type 1 diabetes rat model and correlation with IENFD wasn't present in HFD induced type 2 diabetes mouse model

Langerhans cell (LC) density has been quantified and assessed in different models of neuropathic pain including sciatic nerve injury and STZ induced type 1 diabetic neuropathy, where a significant increase in LC density in rodents with neuropathy and neuropathic pain compared to control healthy animals was observed (Hseieh et al., 1996; Stankovic et al., 1999; Lin et al., 2001; Lindenlaub and Sommer, 2002; Lauria et al., 2005). This literature supports the significant increase in LC density found in the STZ type 1 diabetes rat tissue in this study (figure 17). There was a statistically significant increase in the density of LCs between control and STZ treated type 1 diabetic rats at all timepoints ($p= <.001$). However, this increase wasn't replicated in the HFD (42% and 60%) type 2 diabetic mouse model (figure 28), and further no significant difference was found between the male and female mice fed the same equivalent diet ($p>0.05$). Although there was a small increase in LC density as the fat percentage of the diets increased from control chow to 42% to 60% fat, no significant increase was found ($p>0.05$). This difference across models raises the question whether the cause of the increases in LC density was as result of the direct single i.p. administration of STZ and not the skin peripheral neuropathy. This seems unlikely, however, as an increase in LC density has been reported in various models of neuropathic pain including non STZ diabetic induced (Hsieh et al., 1996; Lindenlaub & Sommer, 2002). It is possible that different pathogeneses have different effects on skin denervation as a study using a neurotoxic-induced neuropathy did not influence the LC density (Lauria et al., 2005). The increase in LC density seen in the STZ induced type 1 diabetic rat model might reflect an upregulation of PGP 9.5 caused by skin denervation or an increase in the number of cytokines present which allow the LCs to mature and produce PGP 9.5, or both (Hamzeh et al., 2002). A separate study found that that an increase in LC density alone did not alter paw withdrawal thresholds, suggesting that LCs do not play a direct role in the generation of hyperalgesia and/or allodynia but can still serve as a useful objective translational biomarker of peripheral neuropathy across species (Lindenlaub and Sommer, 2002).

Correlation analysis of the STZ induced type 1 diabetic model data showed that the increase in LC density and decrease in IENFD were highly negatively inversely correlated ($r= -0.6214$, $p= <0.002$) (Figure 19). Figure 19 also further illustrates that control rats were more likely to have a low number of LCs and a higher number of IENFs compared to STZ treated type 1 diabetic rats. Whereas in the HFD induced type 2 diabetes mice model no correlation between IENFD and LC density was indicated ($p=0.255$, $r^2=0.079$) (figure 29). These correlative analyses support the use of IENF quantification in conjunction with LC density as outcome measurements in certain experimental models of neuropathies.

4.5 Proportional changes in cGRP immunoreactive nerve fibres in Type 1 rat model

Skin innervation is a dynamic process and changes in overall nerve fibre density have been observed. Peptidergic nerve fibres also express TrkA, a receptor for nerve growth factor (NGF), which regulates neuropeptide expression. NGF-Trka signalling pathway has been implicated in pain generation and maintenance through changes in expression of peptides and receptors such as cGRP (Evans et al, 2012). These changes could potentially be used as an objective measure to identify and confirm the type and progression of pathological process such as neuropathic pain. In this study it was shown that in STZ induced type 1 diabetic Wister Han ISG rats there was a significant increase in the percentage of cGRP reactive fibres as a proportion of the total number of IENFs present in diabetic tissue compared to control. There was a significant increase in the percentage of IENFs immunoreactive to cGRP at 2 weeks from 5.7% in controls to 13.1% in STZ induced type 1 diabetic rats ($p=0.012$); at 4 weeks, from 5.6% in controls and 8.69% in STZ induced type 1 diabetic rats, and at 7 weeks, from 6.7% in controls and 9.1% in STZ induced type 1 diabetic rats (figure 22). These observations are in line with the increase in cGRP reactivity found in a chronic itch rat model and a STZ induced type 1 diabetic rat model of neuropathic pain (Evans et al., 2012; Schüttenhelm et al., 2015). It is possible that the increased cGRP labelling is due to elevated cutaneous NGF which is known to modulate cGRP expression (Giniatullin, Nistri & Fabbretti, 2008). Previous studies support this notion highlighting an increase in cGRP reactivity in IENFs in painful but not painless diabetic neuropathy (Karanth et al., 1990; Averill et al., 1995).

Conversely there were no significant differences found when looking at the percentage of cGRP reactive fibres as a proportion of the total number of IENFs present in HFD diet induced type 2 diabetic tissue between male and female mice and the different diet groups (figure 30). There was a slight increase in cGRP reactivity the higher the fat content chow the rats were eating however it was very marginal and not significant ($p>0.05$). As there was a change in overall IENFD, if the presumption that there is an increase in cGRP reactivity in diabetes is true, we would expect to observe an increase in cGRP reactivity in these samples, which wasn't the case. Though (as discussed for LCs) it is possible that there was no change in cGRP due to lower levels of neuropathy (IENF) and neuropathic pain (mechanical/thermal allodynia) exhibited by these diabetic mice, there is also debate in the literature on the correlation between neuropathic pain and cGRP levels. Importantly this has been highlighted in human studies in complex regional pain syndrome finding no correlation between the level of neuropathic pain and cGRP levels (Birklein, Schmelz, Schifter, & Weber, M. 2001; Schinkel 2009). Whereas a study in 2011 investigating cGRP levels in epidermal keratinocytes in 5 patients with post-herpetic neuralgia, 5 patients with diabetes (type mot specified) and 11 age and gender matched controls, found increased cGRP levels in post-herpetic neuralgia compared to control and higher levels of cGRP in painful areas of the skin compared to non-painful (Hou et al., 2011). In a more recent 2020 study, patients who suffered from migraines and peripheral neuropathy and were treated with an anti-cGRP antibody showed a 40% decrease in score on the neuropathy pain scale (Kang & Govindarajan, 2021). Indicating modulation of cGRP correlated with pain relief. This conflicting evidence displays how the relationship between cGRP, and neuropathic pain is not straightforward and warrants further investigation.

In this study cGRP was stained for to show the possibility of cGRP as a molecular biomarker of neuropathic pain but also to differentially stain peptidergic nerve fibres to see if there was altered expression in these compared to the total amount of nerve fibres. It was originally assumed that all peptidergic fibres expressed cGRP, however it has since been demonstrated that 62% of peptidergic fibre population do not express cGRP (Davis et al., 1997; Evans et al., 2012). Studies have also shown that the distinction between peptidergic and non-peptidergic fibres is less clean cut, with there being an overlap between the two (Fang et al., 2006). Increased levels of peptidergic nerve fibres

may be able to distinguish between painful and painless neuropathy and hence a better method to differentiate between the two is needed.

4.6 Lack of VEGF signal in western blot

VEGF plays an important physiological role in the eye under normal conditions; however, it can be upregulated in diabetes causing hyperpermeability of retinal capillaries and migration and proliferation of the retinal endothelial cells, leading to diabetic retinopathy (Alon et al., 1995). To assess the potential changes in VEGF levels in STZ diabetic animals, retinal proteins were quantified using western blot and a primary anti-VEGF antibody. No signals were present when a VEGF antibody was used in any of the sample lanes (figure 23). It would have been expected that VEGF would have been present in all samples, at least at some level. Making it likely that there was issue with the antibody used or the protocol. As protein transfer from the SDS gel to the membrane (blot) was confirmed by signals being present when a GADPH antibody was applied (figure 23), it is most likely that the issue was with the VEGF antibody. This issue could have arisen for multiple reasons. Firstly, there was too little antibody used or the exposure time to the antibody was too short. It is also possible that the antigen was masked by a blocking buffer. Unfortunately, due to time constraints the western blot was only able to be run once so these procedural changes to the antibody use couldn't be tested. The VEGF antibody itself may have become inactive due to repetitive freeze/thawing cycles, however this is unlikely as it was aliquoted on arrival and stored appropriately. The signal strength from GAPDH differed between the lanes, suggesting there was inconsistent amounts of protein loaded into each well.

4.7 Future work

Quantification of IENFs has shown to be a reliable biomarker of neuropathy in a model of type 1 and type 2 diabetes, and the counting method adopted in this study has validity. However, the counts of IENFD were higher than observed in previous studies. Hence, to assess the robustness and rigour of the counting methods at least one additional investigator should independently follow these counting approaches, determining the IENFs, LC density, cGRPs reactivity for consistency.

Given the differences and trends observed in IENFDs between male and female mice in the HFD type 2 diabetic model it would improve translatability and reproducibility of the STZ type 1 diabetic rat model if both females and males were used. This would increase the diversity in experimental design and allow for the important comparisons to be made between the sexes and allow the evaluation of differential changes in biomarkers which could identify why there is a higher occurrence of neuropathic pain in females in the general population. Furthermore, recent recommendation from the MRC state that sex to be "specified and justified in the experimental design of grant applications involving animals, and human and animal tissues and cells" (Guidance for applicants 2022 - Research Councils UK).

As an increase in LCs was only found in the STZ type 1 diabetic rat model and wasn't present in the HFD type 2 mouse model, it is possible that the increase was as a result of the STZ administration and not due to neuropathy. Further investigation using different animal models of neuropathic pain, such as chemotherapy induced (oxaliplatin), chronic constriction injury (CCI) would further allude to the suitability of LCs being used as a biomarker for neuropathy and neuropathic pain.

Due to the change in CGRP being inconsistent between the type 1 and type 2 model, increasing in the STZ model and not changing in the HFD model, the effectiveness of CGRP as a biomarker of

neuropathy was inconclusive in this study. Further investigation in future studies would be warranted due to the potential analgesic therapeutic effect this target has shown (Kang & Govindarajan, 2021). It would also be of added value to assess peptidergic fibres by a means other than CGRP, as a more representative value of the total number of these fibres present and how their expression level changes in neuropathy and in the development of neuropathic pain.

4.8 Conclusions

This study demonstrated that the quantification of IENFD can be reliably and comparatively measured in plantar skin of healthy and diabetic type 1 and 2 neuropathic rodents supporting the usefulness of IENFD quantification as an outcome measurement to assess the development of neuropathy and neuropathic pain in preclinical and clinical models. The observed increase in LC expression levels in the epidermis suggests that this can also be used as an objective biomarker for neuropathy. In combination IENFD and LC density have the potential to assess the development and potential severity of the neuropathy, as well as predict the extent of neuropathic pain and sex differences. The use of CGRP as a reliable biomarker was inconclusive in this study as an observable change was only apparent in the STZ type 1 diabetic rat model and not in the type 2 diabetic mouse model. Further investigation is warranted into its use as a translatable neuropathy biomarker, as well as the role it plays in the generation of neuropathic pain, and mechanism for analgesia.

References

Alon, T., Hemo, I., Itin, A., Pe'er, J., Stone, J., & Keshet, E. (1995). Vascular endothelial growth factor acts as a survival factor for newly formed retinal vessels and has implications for retinopathy of prematurity. *Nature medicine*, *1*(10), 1024-1028.

Andreasen, L. J., Kirk, R. K., Fledelius, C., Yorek, M. A., Lykkesfeldt, J., & Akerstrom, T. (2020). Insulin Treatment Attenuates Small Nerve Fiber Damage in Rat Model of Type 2 Diabetes. *Journal of Diabetes Research*, *2020*.

Arimura, A., Deguchi, T., Sugimoto, K., Uto, T., Nakamura, T., Arimura, Y., et al. (2013). Intraepidermal nerve fibre density and nerve conduction study parameters correlate with clinical staging of diabetic polyneuropathy. *Diabetes research and clinical practice*, *99*(1), 24-29.

Averill, S., McMahon, S. B., Clary, D. O., Reichardt, L. F., & Priestley, J. V. (1995). Immunocytochemical localization of trkA receptors in chemically identified subgroups of adult rat sensory neurons. *European Journal of Neuroscience*, *7*(7), 1484-1494.

Basbaum, A. I., Bautista, D. M., Scherrer, G., & Julius, D. (2009). Cellular and molecular mechanisms of pain. *Cell*, *139*(2), 267-284.

Beiswenger, K. K., Calcutt, N. A., & Mizisin, A. P. (2008). Epidermal nerve fibre quantification in the assessment of diabetic neuropathy. *Acta histochemica, 110*(5), 351-362.

Biomarkers Definitions Working Group, Atkinson Jr, A. J., Colburn, W. A., DeGruttola, V. G., DeMets, D. L., Downing, G. J., et al. (2001). Biomarkers and surrogate endpoints: preferred definitions and conceptual framework. *Clinical pharmacology & therapeutics*, *69*(3), 89-95.

Birklein, F., Schmelz, M., Schifter, S. A., & Weber, M. (2001). The important role of neuropeptides in complex regional pain syndrome. *Neurology*, *57*(12), 2179-2184.

Bönhof, G. J., Strom, A., Püttgen, S., Ringel, B., Brüggemann, J., Bódis, K., et al. (2017). Patterns of cutaneous nerve fibre loss and regeneration in type 2 diabetes with painful and painless polyneuropathy. *Diabetologia*, *60*(12), 2495-2503.

Bouhassira, D., Lantéri-Minet, M., Attal, N., Laurent, B., & Touboul, C. (2008). Prevalence of chronic pain with neuropathic characteristics in the general population. *Pain*, *136*(3), 380-387.

Calandre, E. P., Rico-Villademoros, F., & Slim, M. (2016). Alpha2delta ligands, gabapentin, pregabalin and mirogabalin: a review of their clinical pharmacology and therapeutic use. *Expert review of neurotherapeutics*, *16*(11), 1263-1277.

Calder, J. S., Holten, I., & McAllister, R. M. R. (1998). Evidence for immune system involvement in reflex sympathetic dystrophy. *Journal of hand surgery*, *23*(2), 147-150.

Casanova-Molla, J., Morales, M., Planas-Rigol, E., Bosch, A., Calvo, M., Grau-Junyent, J. M., & Valls-Solé, J. (2012). Epidermal Langerhans cells in small fiber neuropathies. *PAIN®*, *153*(5), 982-989.

Cavalli, E., Mammana, S., Nicoletti, F., Bramanti, P., & Mazzon, E. (2019). The neuropathic pain: an overview of the current treatment and future therapeutic approaches. *International Journal of Immunopathology and Pharmacology*, *33*, 1-10

Cheung, A., Podgorny, P., Martinez, J. A., Chan, C., & Toth, C. (2015). Epidermal axonal swellings in painful and painless diabetic peripheral neuropathy. *Muscle & nerve, 51*(4), 505-513.

Colloca, L., Ludman, T., Bouhassira, D., Baron, R., Dickenson, A. H., Yarnitsky, D., et al. (2017). Neuropathic pain. *Nature reviews Disease primers*, *3*(1), 1-19.

Costa, P. Z., & Soares, R. (2013). Neovascularization in diabetes and its complications. Unraveling the angiogenic paradox. *Life sciences*, *92*(22), 1037-1045.

Cruccu, G., & Truini, A. (2017). A review of neuropathic pain: from guidelines to clinical practice. *Pain and therapy*, *6*(1), 35-42.

Dalsgaard, C. J., Rydh, M., & Haegerstrand, A. (1989). Cutaneous innervation in man visualized with protein gene product 9.5 (PGP 9.5) antibodies. *Histochemistry*, *92*(5), 385-390.

Davis, B. M., Fundin, B. T., Albers, K. M., Goodness, T. P., Cronk, K. M., & Rice, F. L. (1997). Overexpression of nerve growth factor in skin causes preferential increases among innervation to specific sensory targets. *Journal of Comparative Neurology*, *387*(4), 489-506.

Deguchi, T., Hashiguchi, T., Horinouchi, S., Uto, T., Oku, H., Kimura, K., et al., (2009). Serum VEGF increases in diabetic polyneuropathy, particularly in the neurologically active symptomatic stage. *Diabetic Medicine*, *26*(3), 247-252.

Derry, S., Bell, R. F., Straube, S., Wiffen, P. J., Aldington, D., & Moore, R. A. (2019). Pregabalin for neuropathic pain in adults. *Cochrane Database of Systematic Reviews*, (1).

Derry, S., Wiffen, P. J., Moore, R. A., & Quinlan, J. (2014). Topical lidocaine for neuropathic pain in adults. *Cochrane database of systematic reviews*, (7).

Doth, A. H., Hansson, P. T., Jensen, M. P., & Taylor, R. S. (2010). The burden of neuropathic pain: a systematic review and meta-analysis of health utilities. *Pain®*, *149*(2), 338-344.

Dubin, A. E., & Patapoutian, A. (2010). Nociceptors: the sensors of the pain pathway. *The Journal of clinical investigation*, *120*(11), 3760-3772.

Dunnigan, S. K., Ebadi, H., Breiner, A., Katzberg, H. D., Lovblom, L. E., Perkins, B. A., et al. (2013). Conduction slowing in diabetic sensorimotor polyneuropathy. *Diabetes Care*, *36*(11), 3684-3690.

Dworkin, R. H., O'connor, A. B., Backonja, M., Farrar, J. T., Finnerup, N. B., Jensen, T. S., et al. (2007). Pharmacologic management of neuropathic pain: evidence-based recommendations. *Pain*, *132*(3), 237-251.

Evans, L., Andrew, D., Robinson, P., Boissonade, F., & Loescher, A. (2012). Increased cutaneous NGF and CGRP-labelled trkA-positive intra-epidermal nerve fibres in rat diabetic skin. *Neuroscience letters*, *506*(1), 59-63.

Fang, X., Djouhri, L., McMullan, S., Berry, C., Waxman, S. G., Okuse, K., et al., (2006). Intense isolectin-B4 binding in rat dorsal root ganglion neurons distinguishes C-fiber nociceptors with broad action potentials and high Nav1. 9 expression. *Journal of Neuroscience*, *26*(27), 7281-7292.

Field, M. J., McCleary, S., Hughes, J., & Singh, L. (1999). Gabapentin and pregabalin, but not morphine and amitriptyline, block both static and dynamic components of mechanical allodynia induced by streptozocin in the rat. *Pain*, *80*(1-2), 391-398.

Fisher, A. S., Lanigan, M. T., Upton, N., & Lione, L. A. (2021). Preclinical Neuropathic Pain Assessment; the Importance of Translatability and Bidirectional Research. *Frontiers in Pharmacology*, 2308.

Gardell, L. R., Wang, R., Burgess, S. E., Ossipov, M. H., Vanderah, T. W., Malan, T. P., et al. (2002). Sustained morphine exposure induces a spinal dynorphin-dependent enhancement of excitatory transmitter release from primary afferent fibres . *Journal of Neuroscience*, *22*(15), 6747-6755

Gibbins, I. L., Furness, J. B., & Costa, M. (1987). Pathway-specific patterns of the co-existence of substance P, calcitonin gene-related peptide, cholecystokinin and dynorphin in neurons of the dorsal root ganglia of the guinea-pig. *Cell and tissue research*, *248*(2), 417-437.

Gibran, N. S., Jang, Y. C., Isik, F. F., Greenhalgh, D. G., Muffley, L. A., Underwood, R. A., et al. (2002). Diminished neuropeptide levels contribute to the impaired cutaneous healing response associated with diabetes mellitus. *Journal of Surgical Research*, *108*(1), 122-128.

Giniatullin, R., Nistri, A., & Fabbretti, E. (2008). Molecular mechanisms of sensitization of pain-transducing P2X3 receptors by the migraine mediators CGRP and NGF. *Molecular neurobiology*, *37*(1), 83-90.

Gould, J. (2018). Superpowered skin. *Nature*, *563*(7732), S84-S84.

Grandoso, L., Pineda, J., & Ugedo, L. (2004). Comparative study of the effects of desipramine and reboxetine on locus coeruleus neurons in rat brain slices. *Neuropharmacology*, *46*(6), 815-823.

Griffin, J. W., McArthur, J. C., & Polydefkis, M. (2001). Assessment of cutaneous innervation by skin biopsies. *Current opinion in neurology*, *14*(5), 655-659.

Guidance for applicants 2022 - Research Councils UK. Retrieved September 29, 2022. https://www.ukri.org/wpcontent/uploads/2022/07/UKRI-08072022-Guidance-for-Applicants-22.2-FINAL.p

Hamzeh, H., Gaudillere, A., Sabido, O., Tchou, I., Lambert, C., Schmitt, D., et al., (2000). Expression of PGP9. 5 on Langerhans' cells and their precursors. *ACTA DERMATOVENEREOLOGICA-STOCKHOLM-*, *80*(1), 14-16.

Hosoi, J., Murphy, G. F., Egan, C. L., Lerner, E. A., Grabbe, S., Asahina, A., & Granstein, R. D. (1993). Regulation of Langerhans cell function by nerves containing calcitonin gene-related peptide. *Nature*, *363*(6425), 159-163.

Hossain, M. J., Kendig, M. D., Wild, B. M., Issar, T., Krishnan, A. V., Morris, M. J., et al., (2020). Evidence of altered peripheral nerve function in a rodent model of diet-induced prediabetes. *Biomedicines*, *8*(9), 313.

Hou, Q., Barr, T., Gee, L., Vickers, J., Wymer, J., Borsani, E., et al. (2011). Keratinocyte expression of calcitonin gene-related peptide β: implications for neuropathic and inflammatory pain mechanisms. *Pain*, *152*(9), 2036-2051.

Hsieh, S. T., Choi, S., Lin, W. M., Chang, Y., Mcarthur, J. C., & Griffin, J. W. (1996). Epidermal denervation and its effects on keratinocytes and Langerhans cells. *Journal of neurocytology*, *25*(1), 513-524.

Hulse, R. P., Beazley-Long, N., Ved, N., Bestall, S. M., Riaz, H., Singhal, P., et al. (2015). Vascular endothelial growth factor-A165b prevents diabetic neuropathic pain and sensory neuronal degeneration. *Clinical Science*, *129*(8), 741-756.

Hunziker, M. E., Suehs, B. T., Bettinger, T. L., & Crismon, M. L. (2005). Duloxetine hydrochloride: a new dual-acting medication for the treatment of major depressive disorder. *Clinical therapeutics*, *27*(8), 1126-1143.

Jensen, T. S., Backonja, M. M., Jiménez, S. H., Tesfaye, S., Valensi, P., & Ziegler, D. (2006). New perspectives on the management of diabetic peripheral neuropathic pain. *Diabetes and Vascular Disease Research*, *3*(2), 108-119.

Ji, R. R., Kohno, T., Moore, K. A., & Woolf, C. J. (2003). Central sensitization and LTP: do pain and memory share similar mechanisms?. *Trends in neurosciences*, *26*(12), 696-705.

Julius, D., & Basbaum, A. I. (2001). Molecular mechanisms of nociception. *Nature*, *413*(6852), 203-210.

Kang, S. A., & Govindarajan, R. (2021). Anti-calcitonin gene–related peptide monoclonal antibodies for neuropathic pain in patients with migraine headache. *Muscle & Nerve*, *63*(4), 563-567.

Karanth, S. S., Springall, D. R., Francavilla, S., Mirrlees, D. J., & Polak, J. M. (1990). Early increase in CGRP-and VIP-immunoreactive nerves in the skin of streptozotocin-induced diabetic rats. *Histochemistry*, *94*(6), 659-666.

Kennedy, W. R., Wendelschafer-Crabb, G., & Johnson, T. (1996). Quantitation of epidermal nerves in diabetic neuropathy. *Neurology*, *47*(4), 1042-1048.

Khan, M. A. B., Hashim, M. J., King, J. K., Govender, R. D., Mustafa, H., & Al Kaabi, J. (2020). Epidemiology of type 2 diabetes–global burden of disease and forecasted trends. *Journal of epidemiology and global health*, *10*(1), 107.

Koskinen, M., Hietaharju, A., Kyläniemi, M., Peltola, J., Rantala, I., Udd, B., et al. (2005). A quantitative method for the assessment of intraepidermal nerve fibres in small–fibre neuropathy. *Journal of neurology*, *252*(7), 789-794.

Lai, J., Porreca, F., Hunter, J. C., & Gold, M. S. (2004). Voltage-gated sodium channels and hyperalgesia. *Annual review of pharmacology and toxicology*, *44*(1), 371-397.

Lauria, G., Cornblath, D. R., Johansson, O., McArthur, J. C., Mellgren, S. I., Nolano, M., et al. (2005). EFNS guidelines on the use of skin biopsy in the diagnosis of peripheral neuropathy. *European journal of neurology*, *12*(10), 747-758.

Lauria, G., Lombardi, R., Borgna, M., Penza, P., Bianchi, R., Savino, C., ... & Cavaletti, G. (2005). Intraepidermal nerve fiber density in rat foot pad: neuropathologic–neurophysiologic correlation. *Journal of the Peripheral Nervous System*, *10*(2), 202-208.

Lenzen, S. (2008). The mechanisms of alloxan-and streptozotocin-induced diabetes. *Diabetologia*, *51*(2), 216-226.

Levy, D. M., Karanth, S. S., Springall, D. R., & Polak, J. (1989). Depletion of cutaneous nerves and neuropeptides in diabetes mellitus: an immunocytochemical study. *Diabetologia*, *32*(7), 427-433.

Lin, Y. W., Tseng, T. J., Lin, W. M., & Hsieh, S. T. (2001). Cutaneous nerve terminal degeneration in painful mononeuropathy. *Experimental neurology*, *170*(2), 290-296.

Lindenlaub, T., & Sommer, C. (2002). Epidermal innervation density after partial sciatic nerve lesion and pain-related behavior in the rat. *Acta neuropathologica*, *104*(2), 137-143.

Lowy, D. B., Makker, P. G., & Moalem-Taylor, G. (2021). Cutaneous neuroimmune interactions in peripheral neuropathic pain states. *Frontiers in Immunology*, *12*, 660203.

Meacham, K., Shepherd, A., Mohapatra, D. P., & Haroutounian, S. (2017). Neuropathic pain: central vs. peripheral mechanisms. *Current pain and headache reports*, *21*(6), 1-11.

Merskey, H. E. (1986). Classification of chronic pain: Descriptions of chronic pain syndromes and definitions of pain terms. *Pain*.

Misery, L. (1998). Langerhans cells in the neuro-immuno-cutaneous system. *Journal of neuroimmunology*, *89*(1-2), 83-87.

Mittal, S. O., Safarpour, D., & Jabbari, B. (2016). Botulinum toxin treatment of neuropathic pain. *Thieme Medical Publishers: Seminars in neurology*, *36*(1), 73-83.

Mizisin, A. P., Kalichman, M. W., Garrett, R. S., & Dines, K. C. (1998). Tactile hyperesthesia, altered epidermal innervation and plantar nerve injury in the hindfeet of rats housed on wire grates. *Brain research*, *788*(1-2), 13-19.

Mogil, J. S. (2009). Animal models of pain: progress and challenges. *Nature Reviews Neuroscience*, *10*(4), 283-294.

Murphy, D., Lester, D., Clay Smither, F., & Balakhanlou, E. (2020). Peripheral neuropathic pain. *NeuroRehabilitation*, (Preprint), 1-19.

Narayanaswamy, H., Facer, P., Misra, V. P., Timmers, M., Byttebier, G., Meert, T., et al. (2012). A longitudinal study of sensory biomarkers of progression in patients with diabetic peripheral neuropathy using skin biopsies. *Journal of Clinical Neuroscience*, *19*(11), 1490-1496.

National Institute for Health and Care Excellence. (2013). *Neuropathic pain in adults: pharmacological management in non-specialist settings* [CG173]. https://www.nice.org.uk/guidance/cg173

Nolano, M., Simone, D. A., Wendelschafer-Crabb, G., Johnson, T., Hazen, E., & Kennedy, W. R. (1999). Topical capsaicin in humans: parallel loss of epidermal nerve fibres and pain sensation. *Pain*, *81*(1-2), 135-145.

O'Brien, P. D., Guo, K., Eid, S. A., Rumora, A. E., Hinder, L. M., Hayes, J. M., et al., (2020). Integrated lipidomic and transcriptomic analyses identify altered nerve triglycerides in mouse models of prediabetes and type 2 diabetes. *Disease models & mechanisms*, *13*(2), dmm042101.

Obrosova, I.G. (2009) Diabetic painful and insensate neuropathy: pathogenesis and potential treatments. Neurotherapeutics. 6(4), 638-47.

Pawson, E. J., Duran-Jimenez, B., Surosky, R., Brooke, H. E., Spratt, S. K., Tomlinson, D. R., et al., (2010). Engineered Zinc Finger Protein–Mediated VEGF-A Activation Restores Deficient VEGF-A in Sensory Neurons in Experimental Diabetes. *Diabetes*, *59*(2), 509-518.

Percie du Sert, N., & Rice, A. S. C. (2014). Improving the translation of analgesic drugs to the clinic: animal models of neuropathic pain. *British journal of pharmacology*, *171*(12), 2951-2963.

Periquet, M. I., Novak, V., Collins, M. P., Nagaraja, H. N., Erdem, S., Nash, S. M., et al., (1999). Painful sensory neuropathy: prospective evaluation using skin biopsy. *Neurology*, *53*(8), 1641-1641.

Pittenger, G. L., Ray, M., Burcus, N. I., McNulty, P., Basta, B., & Vinik, A. I. (2004). Intraepidermal nerve fibres are indicators of small-fibre neuropathy in both diabetic and nondiabetic patients. *Diabetes care*, *27*(8), 1974-1979.

Polydefkis, M., Griffin, J. W., & McArthur, J. (2003). New insights into diabetic polyneuropathy. Jama, 290(10), 1371-1376.

Provitera, V., Nolano, M., Stancanelli, A., Caporaso, G., Vitale, D. F., & Santoro, L. (2015). Intraepidermal nerve fiber analysis using immunofluorescence with and without confocal microscopy. *Muscle & Nerve*, *51*(4), 501-504.

Quattrini, C., Tavakoli, M., Jeziorska, M., Kallinikos, P., Tesfaye, S., Finnigan, J., et al. (2007). Surrogate markers of small fibre damage in human diabetic neuropathy. *Diabetes*, *56*(8), 2148-2154.

Raja, S. N., Carr, D. B., Cohen, M., Finnerup, N. B., Flor, H., Gibson, S., et al. (2020). The revised IASP definition of pain: concepts, challenges, and compromises. *Pain*, *161*(9), 1976.

Rasband, W.S., ImageJ, U. S. National Institutes of Health, Bethesda, Maryland, USA, https://imagej.nih.gov/ij/, 1997-2018

Ribeiro, S. C., Kennedy, S. E., Smith, Y. R., Stohler, C. S., & Zubieta, J. K. (2005). Interface of physical and emotional stress regulation through the endogenous opioid system and μ-opioid receptors. *Progress in Neuro-Psychopharmacology and Biological Psychiatry*, *29*(8), 1264-1280.

Risher, W. C., & Eroglu, C. (2020). Emerging roles for α2δ subunits in calcium channel function and synaptic connectivity. *Current opinion in neurobiology*, *63*, 162-169.

Rumora, A. E., LoGrasso, G., Hayes, J. M., Mendelson, F. E., Tabbey, M. A., Haidar, J. A., et al., (2019). The divergent roles of dietary saturated and monounsaturated fatty acids on nerve function in murine models of obesity. *Journal of Neuroscience*, *39*(19), 3770-3781.

Sandkuhler, J. (2009). Models and mechanisms of hyperalgesia and allodynia. *Physiological reviews*, *89*(2), 707-758.

Schinkel, C., Scherens, A., Köller, M., Roellecke, G., Muhr, G., & Maier, C. (2009). Systemic inflammatory mediators in post-traumatic complex regional pain syndrome (CRPS I)-longitudinal investigations and differences to control groups. *European journal of medical research*, *14*(3), 130-135.

Schüttenhelm, B. N., Duraku, L. S., Dijkstra, J. F., Walbeehm, E. T., & Holstege, J. C. (2015). Differential changes in the peptidergic and the non-peptidergic skin innervation in rat models for inflammation, dry skin itch, and dermatitis. *Journal of Investigative Dermatology*, *135*(8), 2049-2057.

Shillo, P., Yiangou, Y., Donatien, P., Greig, M., Selvarajah, D., Wilkinson, I. D., et al. (2021). Nerve and vascular biomarkers in skin biopsies differentiate painful from painless peripheral neuropathy in type 2 diabetes. *Frontiers in Pain Research*, *2*.

Shun, C. T., Chang, Y. C., Wu, H. P., Hsieh, S. C., Lin, W. M., Lin, Y. H., et al. (2004). Skin denervation in type 2 diabetes: correlations with diabetic duration and functional impairments. *Brain*, *127*(7), 1593-1605.

Snider, W. D., & McMahon, S. B. (1998). Tackling pain at the source: new ideas about nociceptors. *Neuron*, *20*(4), 629-632.

Sondell, M., Lundborg, G., & Kanje, M. (1999). Vascular endothelial growth factor has neurotrophic activity and stimulates axonal outgrowth, enhancing cell survival and Schwann cell proliferation in the peripheral nervous system. *Journal of Neuroscience*, *19*(14), 5731-5740.

Spindler, B. L., & Ryan, M. (2020). Medications approved for preventing migraine headaches. *The American journal of medicine*, *133*(6), 664-667.

Stankovic, N., Johansson, O., & Hildebrand, C. (1999). Increased occurrence of PGP 9.5-immunoreactive epidermal Langerhans cells in rat plantar skin after sciatic nerve injury. *Cell and tissue research*, *298*(2), 255-260.

Stino, A. M., & Smith, A. G. (2017). Peripheral neuropathy in prediabetes and the metabolic syndrome. *Journal of diabetes investigation*, *8*(5), 646-655.

Sugimoto, K., Baba, M., Suzuki, S., & Yagihashi, S. (2013). The impact of low-dose insulin on peripheral nerve insulin receptor signaling in streptozotocin-induced diabetic rats. *PLoS One*, *8*(8), e74247

Sun, B., Fan, S., Yao, K., Li, Y., & Huang, X. (2018). Changes in intraepidermal nerve fiber and Langerhans cell densities in the plantar skin of rats after mercuric chloride exposure. *Journal of the Peripheral Nervous System*, *23*(1), 17-22.

Surwit, R. S., Kuhn, C. M., Cochrane, C., McCubbin, J. A., & Feinglos, M. N. (1988). Diet-induced type II diabetes in C57BL/6J mice. *Diabetes*, *37*(9), 1163-1167.

Themistocleous, A. C., Ramirez, J. D., Shillo, P. R., Lees, J. G., Selvarajah, D., Orengo, C., et al. (2016). The Pain in Neuropathy Study (PiNS): a cross-sectional observational study determining the somatosensory phenotype of painful and painless diabetic neuropathy. *Pain*, *157*(5), 1132.

Tortora, G.J. and Grabowski, S.R. (2001). Introduction to the human body-the essentials of anatomy and physiology. 5th ed. USA: John Wiley & Sons, Inc. pp.143-144.

Treede, R. D., Rief, W., Barke, A., Aziz, Q., Bennett, M. I., Benoliel, R., et al., (2019). Chronic pain as a symptom or a disease: the IASP Classification of Chronic Pain for the International Classification of Diseases (ICD-11). *pain*, *160*(1), 19-27.

Vader, K., Bostick, G. P., Carlesso, L. C., Hunter, J., Mesaroli, G., Perreault, K., et al., (2021). The revised IASP definition of pain and accompanying notes: considerations for the physiotherapy profession. *Physiotherapy Canada*, *73*(2), 103-106.

Vencappa, S., Donaldson, L. F., & Hulse, R. P. (2015). Cisplatin induced sensory neuropathy is prevented by vascular endothelial growth factor-A. *American journal of translational research*, *7*(6), 1032.

Vincent, A. M., Edwards, J. L., McLean, L. L., Hong, Y., Cerri, F., Lopez, I., et al., (2010). Mitochondrial biogenesis and fission in axons in cell culture and animal models of diabetic neuropathy. *Acta neuropathologica*, *120*(4), 477-489.

von Hehn, C. A., Baron, R., & Woolf, C. J. (2012). Deconstructing the neuropathic pain phenotype to reveal neural mechanisms. *Neuron*, *73*(4), 638-652.

Wang, L., Hilliges, M., Jernberg, T., Wiegleb-Edström, D., & Johansson, O. (1990). Protein gene product 9.5-immunoreactive nerve fibres and cells in human skin. *Cell and tissue research*, *261*(1), 25-33.

Wang, Q., Wu, S., Ding, J., Dong, J. H., & Wang, X. (2019). Loss of cutaneous unmyelinated and myelinated fibers in streptozotocin-induced diabetic rats: a time course study. *Int J Clin Exp Med*, *12*(6), 7038-7046.

Wendelschafer-Crabb, G., Kennedy, W. R., & Walk, D. (2006). Morphological features of nerves in skin biopsies. *Journal of the neurological sciences*, *242*(1-2), 15-21.

Woolf, C. J., & Mannion, R. J. (1999). Neuropathic pain: aetiology, symptoms, mechanisms, and management. *The lancet*, *353*(9168), 1959-1964.

Yam, M. F., Loh, Y. C., Tan, C. S., Khadijah Adam, S., Abdul Manan, N., & Basir, R. (2018). General pathways of pain sensation and the major neurotransmitters involved in pain regulation. *International journal of molecular sciences*, *19*(8), 2164.